

General Comment from Anonymous Referee #1

Li et al. report for the first time the hygroscopic measurements of MBTCA-inorganic system using Raman spectroscopy. The reactions involving HCl(g) release were discussed using the speciation of COOH and COO⁻, and related to the hygroscopic curves obtained by the optical imaging of the nominal particle size. This work would be an important increment to our knowledge of SOA hygroscopicity, but the current version is not ready for publication in ACP because of a number of issues as shown below.

Response: We thank the reviewer very much for the careful evaluation and valuable comments for our work. We revised the manuscript as much as possible respecting the reviewer's comments.

Specific comments from Anonymous Referee #1 (comments are in italic)

** The abstract is rather long. I suggest the authors to make the text more concise by focusing more results and their interpretation.*

Response: We revised the abstract in a more concise way as can be seen in the revised abstract.

** Lines 82-83: It is not clear how MBTCA can accelerate the new particle formation. The authors mentioned that MBTCA is extremely low volatile and one of the SOA components, i.e., one of the particulate compositions. Are you saying that preexisting aerosols enhance the new particle formation?*

Response: As described in the papers (Donahue et al., 2013; Elm, 2019), MBTCA can nucleate the sulfuric acid vapor or provide polar functional groups to form and grow

molecular clusters through hydrogen bonds, which promote the new particle formation. However, as this sentence is not directly related to our work, it was omitted in the revised version without deteriorating the context.

** Line 127: I don't agree with the author's statement that RMS can provide the chemical compositions. RMS detects chemical functional groups of a molecule of interest.*

Response: The reviewer is correct, and the sentence was modified as “RMS can provide information on chemical functional groups, water contents, molecular interactions, and phase states of the aerosol particles” (lines 133-135 in the marked revised version below).

** Lines 170-173: It is useful if the authors show the experimentally measured hygroscopic curves of NaCl together with the thermodynamic model prediction.*

Response: The hygroscopic curve of NaCl (as shown below) was put into the supporting information as Fig S2.

** Why were deposited and levitated particles examined in this study. The authors need to elaborate the necessity of using levitated particles.*

Response: “The deposited particles (~6.5 μm in average in this study) may have some influences from the collecting substrate such as a facilitated heterogeneous nucleation, which can be eliminated in the levitation system due to the substrate-free and contactless properties. However, the particles in the levitation system are generally large in size (~80 μm in average in this study), which is less atmospherically relevant. And thus the analysis of the particles in both systems is expected to give more detailed information on the

hygroscopic behavior of MBTCA aerosols.” This paragraph was added in the revised text (lines 119-125).

** In Figure 2, the authors need to explicitly define the type of MBTCA particles. How do types 1-3 of the particles differ?*

Response: The following argument was added in the marked revised manuscript (lines 271-295). “Specifically, the types of pure MBTCA particles were classified as, “type 1: with a prompt efflorescence at ~50% RH during dehydration; type 2: with a gradual efflorescence at ~35% RH during dehydration; type 3: with a gradual efflorescence at ~37% RH during humidification”, based on their different behavior when efflorescence occurred. The different efflorescence behavior was attributed to different nucleation mechanisms: heterogeneous nucleation for types 1 and 2 particles (seed-containing), and homogeneous nucleation for type 3 particles (pure). MBTCA powders, which was used for making the MBTCA solution, has intrinsic unknown impurity of 2%, and they were used without any purification. When MBTCA powders were dissolved in DI water and particles were generated by the nebulization of the aqueous solution using N₂ gas, impurities were either absent or associated with the droplets. The impurities existed in types 1 and 2 particles after nebulization, acting as seed crystals to induce efflorescence. Aqueous moieties in particles were reported to effloresce more easily by heterogeneous nucleation in the presence of seeds (Schlenker and Martin, 2005; Li et al., 2014; Gupta et al., 2015). The lower ERH and gradual efflorescence of type 2 compared to type 1 particles might be due to the less amount of impurities. Type 3 particles contain negligible or no seed crystals, and large kinetic barrier and/or diffusional resistance make the formation of the crystal structure difficult owing to the decreasing availability of condensed water

during dehydration, so that they did not experience any efflorescence. A similar situation was observed for NH_4NO_3 , NaNO_3 , and NH_4HSO_4 particles (Lightstone et al., 2000; Hoffman et al., 2004; Gibson et al., 2006; Kim et al., 2012; Jing et al., 2018; Sun et al., 2018; Wu et al., 2019b). The Si substrates used in this study could also facilitate efflorescence (Eom et al., 2014; Wang et al., 2017). The efflorescence during humidification like type 3 particles was previously reported for Amazonian rain forest aerosols (Pöhlker et al., 2014) and the laboratory-generated NaCl-MgCl_2 mixture particles (Gupta et al., 2015). Thus, this phenomenon is not rare. And it was claimed that the aerosol particles initially had amorphous or poly-crystalline structures and underwent restructuring through kinetic water and ion mobilization in the presence of sufficient condensed water, resulting in overcoming the kinetic barrier and crystallization during humidification.”

** Line 230: Please provide the evidence of the phase change at $\text{RH} = 36.7\%$. The optical images of type 3 particle in Figure 2 show the morphology change from 34% RH to 36.7% RH, but it does not necessarily mean phase change.*

Response: As shown in the optical image and Raman spectrum in Fig. 2, type 3 particles became irregular in shape during the humidification process, and the overlapped C=O (from COOH) peak at $1660 - 1680 \text{ cm}^{-1}$ entirely shifted to 1660 cm^{-1} when the RH was increased from 34% to 36.7%. Both the morphological and RMS data clearly indicate the phase change from amorphous/solid-state to solid state. The sentence at line 230 was modified as, “type 3 particles experienced a gradual morphological change at $\text{RH} = 34-36.7\%$ and remained the same until $\text{RH} = \sim 85\%$ ”, for the precise expression (line 240 in the marked revised version).

** Lines 250-252: Please clarify if the authors purposely injected impurity in the MBTCA particles. This is related to my earlier question: what is the type?*

Response: The MBTCA powders with intrinsic 2% impurity were used without any purification and no impurity was injected purposely. The information was clarified in the revised text (lines 276-277 in the marked revised version). Regarding the types of the particles, please see the response above.

** Line 270: It is confusing. The implication is based on the previous study or the current study?*

Response: The sentence was modified as, “A previous study showed that MBTCA was not hydrated significantly in the ambient atmosphere (Kildgaard et al., 2018), and our results also implied that the MBTCA stay in the air as solids once they effloresced.” (line 300 in the marked revised version), to avoid the confusion.

** In Figure 3, one of the interesting results is the efflorescence at 46.8% RH during the humidification. The explanation for this phenomenon is rather dry. The authors need to elaborate more. It would be also useful if the authors can discuss the repeatability of such a phenomenon.*

Response: Efflorescence during humidification was previously reported for Amazonian rain forest aerosols (Pöhlker et al., 2014) and the laboratory-generated NaCl–MgCl₂ mixture particles (Gupta et al., 2015). And thus this phenomenon is not rare and it was claimed that the aerosol particles initially had amorphous or poly-crystalline structures and underwent restructuring through kinetic water and ion mobilization in the presence of

sufficient condensed water, resulting in overcoming the kinetic barrier and crystallization during humidification. ← This paragraph was added (lines 290-295 in the marked revised version)

Efflorescence during humidification was also observed for type 3 MBTCA particles, in addition to the observation in Fig. 3 for tri-sodium MBTCA particles, which seemed to be attributed to the similar structure to pure MBTCA particles when all three COOH were replaced by COONa.

** Based on the chemical reactions the current study has proposed, acidic conditions are preferable for the reactions to proceed. However, Figure 7b shows the higher degree of 2 reaction for particles with MBTCA:NaCl = 1:3 than for those with that = 1:1. Particles with the higher abundance of NaCl (MBTCA:NaCl=1:3) are supposed to be less acidic. Do you have any explanation on it?*

Response: The reactions were driven by the liberation of HCl(g), so the increased availability of both dissociated H⁺ and Cl⁻ should facilitate the reaction, which makes the degree of reaction follows the sequence of MBTCA:NaCl = 1:3>1:2>1:1. We did not say that acidic conditions are preferable for the reactions to proceed, instead we said about “the availability”. The H⁺ cannot fully dissociate due to the weak acidic property of MBTCA, and NaCl can be fully consumed only when enough H⁺ is provided, so that the reaction was complete only for the mixtures with MBTCA:NaCl = 2:1 in this study.

** Figure 8a exhibits some heterogeneity of elemental distributions for particles with 1:2 and 1:3, which makes me wonder where Raman spectra were obtained. Raman spectra obtained from the edge and the center of the particles would be different.*

Response: The Raman spectra shown in the figures were all obtained in the center of the particles. However, the Raman spectra were obtained both at the center and the edge of the particles for comparison during the measurement when the heterogeneity appeared. The reviewer is correct in that the spectra from the edge and the center were different, but only in the intensity since NaCl is Raman inactive. As shown in the figure below (which was put into the supporting information as Fig. S3), the Raman spectra which were obtained from the center and edge of an exemplar MBTCA:NaCl = 1:3 particle during the humidification process, match well after normalization to the CH peak at 1460cm^{-1} . The discussion on the Raman spectra was given (lines 398-404 in the marked revised version).

** The levitated particles show the lower reactivity than the deposited particles. The authors ascribed it to less release of HCl and the quenching process, which are too speculative. One more factor I want to point out is the almost one order of magnitude difference of the size between the two particles. It may not affect the reaction rates at a given RH, but it may do the release of HCl. I suggest the authors to discuss the potential size effect on the reactivity difference.*

Response: The default setting of N_2 flow inside the see-through impactor cell and the levitation cell were 4 and $0.2\text{ L}\cdot\text{min}^{-1}$, respectively, so we think that the levitation system is relatively closed compared to the see-through impactor system, which leads to less release of HCl(g) . And the quenching process also dramatically decreases the reaction time due to the crystallization of both organic and inorganic compositions. We agree with the reviewer that the larger size of the levitated particles can also limit the release of HCl (Kerminen et al., 1997). The information was added into the marked revised text (lines 553-557 in the marked revised version).

** Interestingly, when the authors used the levitated particles, no size decrease (i.e., $A/A_0 < 1$) was observed. The authors need to explain it. The size decrease observed with the deposited particles was attributed to the structural rearrange in the main text, but we may be seeing the effect of substrate.*

Response: We think why the shrinkage of the particles before deliquescence was not captured for the levitated particles can be because the size of the particles ($\sim 80\text{ }\mu\text{m}$ in average in this study) is too large for the structural rearrangement to be observed. And the 2-D optical images of the particles were used for plotting the hygroscopic curves even though the particles were levitated, which might lead to some missing information on the 3-D level. ← (lines 534-538 in the marked revised version) We agree with the reviewer that the substrate can also affect the shrinkage. Especially, the hydrophilic substrate (such as Si wafer used in this study) seems to favor this phenomenon (Eom et al., 2014).

References

- Donahue, N. M., Ortega, I. K., Chuang, W., Riipinen, I., Riccobono, F., Schobesberger, S., Dommen, J., Baltensperger, U., Kulmala, M., Worsnop, D. R., and Vehkamäki, H.: How do organic vapors contribute to new-particle formation?, *Faraday Discussions*, 165, 10.1039/c3fd00046j, 2013.
- Elm, J.: Unexpected Growth Coordinate in Large Clusters Consisting of Sulfuric Acid and $\text{C}_8\text{H}_{12}\text{O}_6$ Tricarboxylic Acid, *J Phys Chem A*, 10.1021/acs.jpca.9b00428, 2019.
- Eom, H. J., Gupta, D., Li, X., Jung, H. J., Kim, H., and Ro, C. U.: Influence of collecting substrates on the characterization of hygroscopic properties of inorganic aerosol particles, *Anal Chem*, 86, 2648-2656, 10.1021/ac4042075, 2014.

- Gupta, D., Eom, H. J., Cho, H. R., and Ro, C. U.: Hygroscopic behavior of NaCl–MgCl₂ mixture particles as nascent sea-spray aerosol surrogates and observation of efflorescence during humidification, *Atmospheric Chemistry and Physics*, 15, 11273–11290, 10.5194/acp-15-11273-2015, 2015.
- Kerminen, V.-M., Pakkanen, T. A., and Hillamo, R. E.: Interactions between inorganic trace gases and supermicrometer particles at a coastal site, *Atmospheric Environment*, 31, 2753–2765, 1997.
- Li, X., Gupta, D., Eom, H.-J., Kim, H., and Ro, C.-U.: Deliquescence and efflorescence behavior of individual NaCl and KCl mixture aerosol particles, *Atmos. Environ.*, 82, 36–43, doi:10.1016/j.atmosenv.2013.10.011, 2014.
- Pöhlker, C., Saturno, J., Krüger, M. L., Förster, J.-D., Weigand, M., Wiedemann, K. T., Bechtel, M., Artaxo, P., and Andreae, M. O.: Efflorescence upon humidification? X-ray microspectroscopic in situ observation of changes in aerosol microstructure and phase state upon hydration, *Geophys. Res. Lett.*, 41, 2014GL059409, doi:10.1002/2014gl059409, 2014.
- Schlenker, J. C. and Martin, S. T.: Crystallization Pathways of Sulfate-Nitrate-Ammonium Aerosol Particles, *J. Phys. Chem. A*, 109, 9980–9985, doi:10.1021/jp052973x, 2005.

Figure S2. Hygroscopic curve of a pure NaCl particle. The transition RHs recorded during humidification and dehydration processes are marked with arrows in the hygroscopic curves.

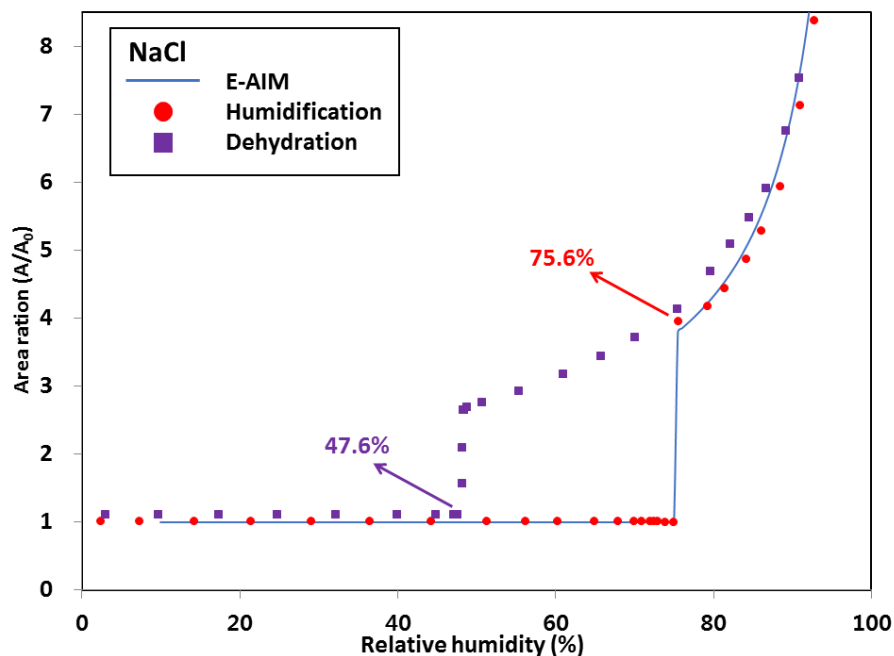
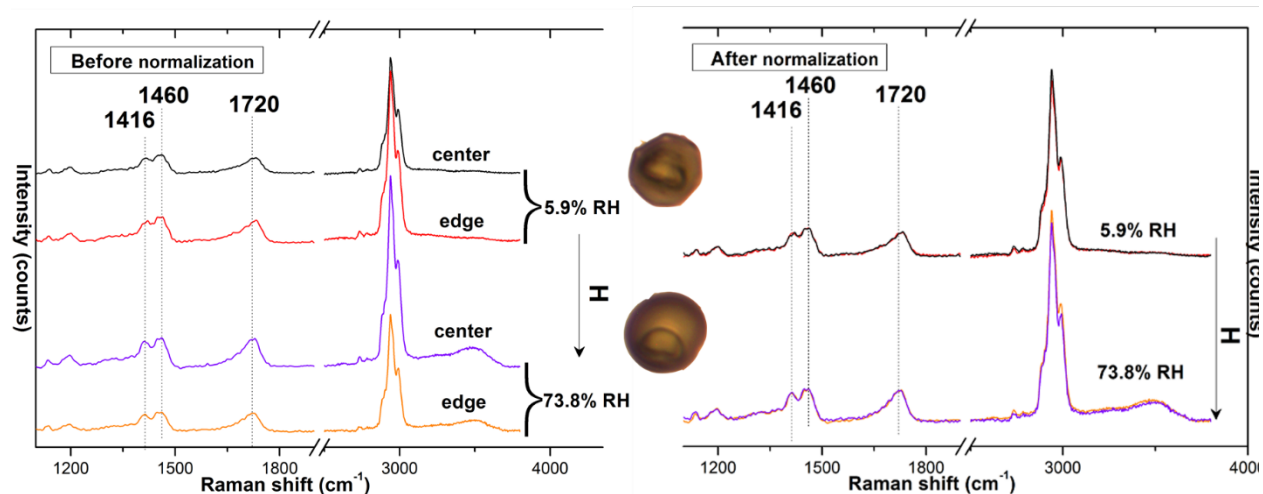


Figure S3. Comparison of Raman spectra of an exemplar particle (MBTCA:NaCl = 1:3) obtained at the center and edge of the particle before and after normalization to the CH peak at 1460 cm^{-1} during humidification (H) process from RH = 5.9% (end of dehydration) to RH = 73.8% (just before deliquescence).



General Comment from Anonymous Referee #2

In this work, the authors investigated the hygroscopicity of laboratory-generated, micrometer-sized, pure MBTCA and its salts using in-situ Raman microspectrometry (RMS). The authors have clearly demonstrated how interactions between the MBTCA and NaCl could modify the aerosol composition and subsequent hygroscopic behaviors during the hygroscopic measurement. The paper is generally well written. I have minor comments and suggestions for authors' consideration before the paper is accepted for publication.

Response: We thank the reviewer very much for the careful evaluation and valuable comments for our work. Here we provide the response to the reviewer's comments.

Specific comments from Anonymous Referee #2 (comments are in italic)

** Line 115, "The particles on the Si wafer were exposed to a hygroscopic measurement cycle, where they experienced dehydration process first (by decreasing RH from ~95 to ~1%), followed by a humidification process (by increasing RH from ~1 to ~95%). Can the authors discuss whether an equilibrium state was achieved in their measurements?"*

Response: During the measurements, each humidity condition (from ~1 to ~95% RH with 1% RH step) was sustained for at least 2 mins in order to provide an enough time for condensing or evaporating of water. As the reaction of MBTCA and NaCl is driven by the gaseous HCl liberation in the open hygroscopic measurement system, the equilibrium cannot be achieved. The information was added in the revised version (lines 174-176 in the marked revised version).

* Line 139, “Mono-/di-/tri-sodium MBTCA salt solutions were obtained by mixing MBTCA and NaOH (>99.9% purity, Sigma-Aldrich) with molar ratios of MBTCA:NaOH = 1:1, 1:2, and 1:3, respectively.” What are the pHs of these aerosols?

Response: The initial pHs of the nebulized aerosol particles should be equal to the solution (0.3 M for all the solutions). The roughly calculated pH values without considering temperature and activity of the chemicals are 2.04, 4.22, 5.82, and 10.16, while the measured pH values are 2.03, 4.07, 5.66, and 10.73 for MBTCA, mono-/di-/tri-sodium MBTCA salt solutions, respectively. The pHs of the aerosols according to RH changes are not available in our study.

* Line 251, “The different behavior of the MBTCA particles can be attributed to different nucleation mechanisms, i.e., homogeneous and heterogeneous nucleation, for pure and impure (seed-containing) MBTCA particles, respectively. A similar situation was reported for NH_4NO_3 , NaNO_3 , and NH_4HSO_4 particles (Lightstone et al., 2000; Hoffman et al., 2004; Gibson et al., 2006; Kim et al., 2012; Jing et al., 2018; Sun et al., 2018; Wu et al., 2019b). The Si substrates used in this study could also facilitate efflorescence (Eom et al., 2014; Wang et al., 2017).” While the authors have provided possible explanations for the different hygroscopic behaviors of MBTCA particles, it would be important to provide more detailed explanation for each hygroscopic behavior. For example, why did type 1 and type 2 aerosols effloresce at different RH? Any reason why type 3 aerosols were being observed in this work?

Response: Please see the response to the Referee #1 regarding the further explanations of particle types.

* Line 284, “ NaH_2M and Na_2HM particles still showed the same shapes and Raman spectra with those at RHs = 3.4% and 2.8%, respectively. These results indicate the non-crystallizable properties and supersaturated amorphous phase state of the particles. The Na_3M particles behaved differently as they did not crystallize during the dehydration process. On the other hand, the aerosols exhibited efflorescence at RH = 46.8% during the humidification process (Fig. 3(c)), deliquesced to become a droplet at RH = 53.1%, and grew continuously after that with increasing RH.” As mentioned above, can the authors comment: Could the crystallization of Na_3M aerosols attribute to the presence of impurities, the use of Si substrates or other factors? Could the authors rule out these possibilities in their measurements? Can the authors also comment: What is the water uptake (e.g. aerosol water content) of mono-/di-/tri-sodium MBTCA salt aerosols? Are they different?

Response: As explained in the paper, the 3 types of pure MBTCA particles with different behavior were observed in the same hygroscopic measurement among 100 particles on the substrate, and crystallization of types 1 and 2 were attributed to the random inclusion of impurity seed particles or the Si wafer substrate, while that of type 3 was due to homogeneous crystallization. However, as for the Na_3M aerosols, all the observed particles on the substrate (around 100 particles) behaved exactly in the same way as shown in the Fig. 3(c) with crystallization during humidification process, similar to the type 3 pure MBTCA particles, so we think the major contribution to the crystallization of Na_3M particles is also homogeneous crystallization, instead of heterogeneous crystallization induced by impurities and Si substrate effect. Please see the response to the Referee #1’s comment which is similar to this comment.

The quantification of the aerosol water content is not available in our study. But based on the water band in the Raman spectra at $\sim 3400\text{ cm}^{-1}$ in Fig. 3, the water content is in the sequence of tri- > di- > mono-sodium MBTCA droplets.

** Figure 4, unlike the pure MBTCA and mono-/di-/tri-sodium MBTCA salt aerosols, why the dehydration and humidification curves of MBTCA:NaCl = 1:1 and 2:1 do not overlap with each other?*

** Figure 5, why the dehydration and humidification curves of MBTCA:NaCl = 1:2 and 1:3 do not overlap with each other after deliquescence?*

Response: These two comments will be responded together. The humidification and dehydration curves of the MBTCA-NaCl mixtures do not overlap with each other mainly due to the different amounts of NaCl in the processes. As shown in the Fig. S2 above, NaCl is quite hygroscopic with around four times change in 2-D area after deliquescence, so the decreased amount of NaCl in the mixtures also lead to the smaller 2-D area when the particles of MBTCA:NaCl = 1:1 and 2:1 and MBTCA:NaCl = 1:2 and 1:3 experienced hygroscopic growth during the humidification process, compared to those before dehydration. The information was added into the text (lines 419-424 in the marked revised version).

** In 3.3.3 Chemical reactivity of aerosols generated from MBTCA–NaCl mixture solutions, the authors have provided a nice discussion of how the chemical composition would evolve due to the chemical reactions between MBTCA and NaCl during the experiments. My question is: do the extent of the reactions depends on the experimental time? Would the duration of the experiments would significantly affect the hygroscopic behaviors observed*

for different systems in the experiments? Since the chemical compositions evolves over time, can the authors discuss whether an equilibrium state was achieved in their hygroscopic measurements?

Response: As responded above, each RH point was sustained for at least 2 mins, but the equilibrium cannot be archived as the measurement system is not closed. It is natural to assume that the experimental time has effects on the reaction extent under the open measurement system. As discussed for the levitation experiment which uses a somewhat more closed system than the see-through impactor system, the reaction extents were smaller than those for the see-through impactor system.

** Line 472, “Two types of hygroscopic behavior of pure MBTCA particles were observed, corresponding closely to types 1 and 3 aerosol particles in the see-through impactor system.” Can the authors further elaborate why type 1 aerosol is observed in levitated pure MBTCA aerosols?*

Response: As described in the paper, the levitated droplets experienced quenching process before the hygroscopic cycle measurement. During the quenching and humidification processes, two types of hygroscopic behavior of pure MBTCA particles were observed, corresponding closely to types 1 and 3 aerosol particles in the see-through impactor system, due to heterogeneous crystallization induced by impurity seed crystals and homogeneous crystallization, respectively. Since the levitation system is substrate-free, the substrate effect is eliminated. The information was added into the text (lines 523-524 in the marked revised version).

Hygroscopic behavior of aerosols generated from solutions of 3-methyl-1,2,3-butanetricarboxylic acid, its sodium salts, and its mixtures with NaCl

Li Wu¹, Clara Becote^{2,3,4}, Sophie Sobanska², Pierre-Marie Flaud^{3,4}, Emilie Perraudin^{3,4}, Eric Villenave^{3,4}, Young-Chul Song¹, Chul-Un Ro^{1*}

¹Department of Chemistry, Inha University, Incheon, South Korea

²Institut des Sciences Moléculaires, UMR CNRS 5255, University of Bordeaux, Talence, France

³University of Bordeaux, EPOC, UMR 5805, 33405 Talence cedex, France

⁴CNRS, EPOC, UMR 5805, 33405 Talence cedex, France

Abstract

MBTCA ~~Secondary organic aerosols (SOAs), which are formed and transformed through complex physicochemical processes in the atmosphere, have attracted considerable attention over the past decades because of their impacts on both climate change and human health. Recently,~~ (3-methyl-1,2,3-butanetricarboxylic acid), a low volatile, highly oxidized, secondary generation product of monoterpenes, is one of the most relevant tracer compounds for biogenic SOAs. ~~Therefore, MBTCA was selected to understand its hygroscopic properties better. In addition, interactions between the organic acid and inorganic components have been reported, which may alter their hygroscopic properties mutually.~~ In this study, laboratory-generated, micrometer-sized, pure MBTCA, mono-/di-/tri-sodium MBTCA salts, and MBTCA-NaCl mixture aerosol particles of four mixing ratios (molar ratios = 1:1, 1:2, 1:3, and 2:1) were examined systematically to observe their hygroscopic behavior by varying the relative humidity (RH) from RH = ~95% to ~1% through a dehydration process, followed by a humidification process from RH = ~1% to ~95%, using in-situ Raman microspectrometry (RMS) assembled with a see-through impactor where the particles were deposited on a Si wafer. The hygroscopic behavior of pure MBTCA and MBTCA-NaCl mixture aerosol particles of three mixing ratios (molar ratios = 1:1, 1:2, and 1:3) were also examined using a levitation system mounted on in-situ RMS through a humidification process from RH

*Corresponding author. Tel.: +82 32 860 7676; Fax: +82 32 867 5604; E-mail: curo@inha.ac.kr

= ~10% to ~80% after a quenching process from droplets, followed by dehydration from RH = ~80% to ~10%. The pure MBTCA droplets effloresced at RH = ~30-57.8% and did not dissolve until RH > 95%. The mono- and di-sodium MBTCA salt aerosols did not show clear efflorescence RH (ERH) and deliquescence RH (DRH). In contrast, the tri-sodium MBTCA salt exhibited ERH = ~44.4-46.8% and DRH = ~53.1%, during the hygroscopic experiment cycle. The mixture aerosols generated from solutions of MBTCA:NaCl = 1:1 and 2:1 showed no visible ERH and DRH in the see-through impactor because of the partial and total consumption of NaCl, respectively, through chemical reactions during the dehydration process. The mixture particles with a 1:1 molar ratio in the levitation system exhibited a clear DRH at ~71% and ERH at ~50%. This suggests less reaction between the mixtures and a larger portion of NaCl remaining in the levitation system. The other mixtures of MBTCA:NaCl = 1:2 and 1:3 displayed single-stage efflorescence and deliquescence at ERH = ~45-50% and DRH = ~74%, respectively, because of the considerable amount of NaCl present in the mixture aerosols in both systems. Observations and Raman analyses indicated that only monosodium MBTCA salt aerosols could be formed through a reaction between MBTCA and NaCl. The reaction occurred more rapidly with a more elevated concentration of either MBTCA or NaCl, and the controlling factor for the reactivity of the mixtures depended mostly on the availability of H⁺ dissociated from the MBTCA tricarboxylic acid. The lower degree of reaction of the mixture particles in the levitation system might be caused by the relatively airtight circumstance inside, i.e., the less release of HCl. In addition, the quenching process, i.e., the starting point of the hygroscopicity experiments, induced the solidification of MBTCA, and further, a slow reaction between MBTCA and NaCl. The study revealed that the interactions between the MBTCA and NaCl could modify the properties of the organic acid in the atmosphere, leading to enhanced capability of the probable heterogeneous chemistry in the aqueous aerosols.

1. Introduction

Chemical processes, such as gas-phase oxidations of airborne biogenic and anthropogenic volatile organic compounds (VOCs) by ozone (O₃), hydroxyl radical (OH), and nitrate radical (NO₃), and their condensed-phase reactions with preexisting aerosols, can promote the formation of increasingly oxidized and less volatile secondary organic aerosols (SOAs). SOAs are a ubiquitous and dominant fraction of the

55 fine aerosol mass that exists as liquid, amorphous solid, semi-solid, and phase-separated aerosol particles
56 (Jang et al., 2002; Hallquist et al., 2009; Jimenez et al., 2009; Virtanen et al., 2010; Koop et al., 2011;
57 Bateman et al., 2015b; Shrivastava et al., 2015; Bernard et al., 2016; Pajunoja et al., 2016; Freedman,
58 2017; Shrivastava et al., 2017; Kim et al., 2018; Srivastava et al., 2018; Liu et al., 2019; Slade et al., 2019;
59 Song et al., 2019; Wu et al., 2019a). These aerosols are of critical importance because of their ability to
60 scatter and absorb solar radiation directly, to affect the number of CCN (cloud condensation nuclei)
61 through the formation of new particles and the growth of preexisting particles, and further impact the
62 climate and human health (Haywood and Boucher, 2000; Topping et al., 2013; Poschl and Shiraiwa, 2015;
63 Reid et al., 2018; Marsh et al., 2019). SOAs are highly dynamic, multiphase chemical systems with a
64 range of volatility and solubility and model simulations have claimed that the phase state of SOAs differs
65 according to the global locations and altitudes with an evolving relative humidity (RH), temperature, and
66 particle composition (Kroll and Seinfeld, 2008; Shiraiwa et al., 2017).

67 Oxidative products of biogenic VOCs, such as monoterpenes (e.g., α - and β -pinenes), act as a
68 dominant source of SOAs as they have high emission rates on a global scale and give considerable SOA
69 yields, and they play a central role in new particle formation (Guenther et al., 1995; Lignell et al., 2013;
70 Mutzel et al., 2016; Holopainen et al., 2017). Carboxylic acid-containing organic compounds comprise a
71 large fraction of SOAs in the Northern Hemisphere (Yatavelli et al., 2015). An extremely low-volatile
72 tricarboxylic acid, 3-methyl-1,2,3-butanetricarboxylic acid (MBTCA, $C_8H_{12}O_6$), has become one of the
73 most relevant tracer compound for terpene SOAs (Jaoui et al., 2005; Szmigielski et al., 2007; Zhang et
74 al., 2010; Donahue et al., 2012; Müller et al., 2012; Lai et al., 2015; Sato et al., 2016). In addition, it is
75 also a few well-known compounds with a high O:C ratio that is formed in the oxidation of VOCs (Dunne
76 et al., 2016). MBTCA is a second or later generation reaction product from monoterpenes by the OH-
77 initiated oxidation of pinonic acid (PA) in the gaseous and aqueous phases and even at the air-water
78 interface (Müller et al., 2012; Praplan et al., 2012; Aljawhary et al., 2016; Enami and Sakamoto, 2016).
79 The MBTCA concentrations were found to be positively correlated with temperature because of the
80 enhanced photochemical production of PA by OH radicals with increasing temperature (Hu et al., 2008;
81 Zhang et al., 2010; Gómez-González et al., 2012; Miyazaki et al., 2012). A further reaction between
82 MBTCA and OH radicals can result in CO_2 loss (Kostenidou et al., 2018). MBTCA can also accelerate

the new particle formation by effectively stabilizing initial molecular clusters with or without sulfuric acid (Donahue et al., 2013; Elm, 2019). MBTCA was first observed at the Amazon basin and in summer aerosols from Ghent, Belgium (Kubátová et al., 2000; Kubátová et al., 2002). The compound was later found in the USA (Jaoui et al., 2005), Europe (Fu et al., 2009; Kourtchev et al., 2009; Zhang et al., 2010; Yasmeen et al., 2011; Gómez-González et al., 2012; Vogel et al., 2013; Kammer et al., 2018; Vlachou et al., 2019), Japan (Miyazaki et al., 2012), the polar regions (Hu et al., 2013), China (Hu et al., 2008; Ding et al., 2012; Li et al., 2013; Fu et al., 2014; Kang et al., 2018; Hong et al., 2019), and Australia (Cui et al., 2019). In addition, it has been observed in forest, marine, mountainous, urban, and rural aerosols, with its levels ranging from 0.03 to 100 ng/m³, and the level was generally higher in the fine particle fraction than in the coarse fraction (Zhang et al., 2010).

The ability of the aerosol particles to uptake water in the air is dependent on one of the most important physicochemical properties, i.e., the hygroscopicity (Jimenez et al., 2009; Chu et al., 2014; Tang et al., 2019). Hygroscopicity can help better understand the (i) aerodynamic properties, (ii) cloud-droplet nucleation efficiency, (iii) optical properties, and (iv) physicochemical changes through complicated heterogeneous chemical reactions of aerosol particles with various atmospheric gas-phase species. MBTCA was predicted to partition significantly into aerosol-liquid-water (ALW) (Aljawhary et al., 2016). Therefore, a study on the hygroscopic behavior of MBTCA is important for understanding its phase states better when it interacts with water vapor at different RHs as well as its impacts on the heterogeneous chemical reactions, atmospheric environment, and human health (Parsons et al., 2004; Mikhailov et al., 2009; Bateman et al., 2015a; Freedman, 2017; Slade et al., 2019). Atmospheric particles typically involve complex internal mixtures of organic and inorganic compounds (Shrivastava et al., 2017; Karadima et al., 2019). The interactions between organic and inorganic compounds may alter the chemical compositions of SOAs, which in turn affect their physicochemical properties, such as hygroscopicity (Rudich et al., 2007; Wu et al., 2011; Wang et al., 2015; Jing et al., 2016; Wang et al., 2018). Dicarboxylic acids (DCAs) can undergo reactions with inorganics, such as NaCl, resulting in Cl depletion and HCl liberation (Ma et al., 2013; Li et al., 2017). On the other hand, the interactions between tricarboxylic acids and inorganics have never been investigated.

110 In this study, in situ Raman microspectrometry (RMS) was used to examine the hygroscopic behavior,
111 evolution of the chemical composition, phase states, and microstructures, and chemical reactivity of
112 laboratory-generated, micrometer-sized aerosols generated from a pure MBTCA solution, mono-/di-/tri-
113 sodium MBTCA salt solutions, and MBTCA-NaCl mixture solutions. RMS was assembled with either a
114 see-through impactor, where the particles were deposited on a Si wafer, or a levitation system. The
115 particles on the Si wafer were exposed to a hygroscopic measurement cycle, where they experienced a
116 dehydration process first (by decreasing RH from ~95 to ~1%), followed by a humidification process (by
117 increasing RH from ~1 to ~95%). The particles in the levitation system experienced a humidification
118 process first (by increasing the RH from ~10 to ~80%) after quenching from droplets, followed by a
119 dehydration process (by decreasing RH from ~80 to ~10%). The deposited particles (~6.5 μm size in
120 average in this study) may have some influences from the collecting substrate such as a facilitated
121 heterogeneous nucleation, which can be eliminated in the levitation system due to the substrate-free and
122 contactless properties. However, the particles in the levitation system are generally large in size (~80 μm
123 in average in this study), which is less atmospherically relevant. And thus, the analysis of the particles in
124 both systems is expected to give more detailed information on the hygroscopic behavior of MBTCA
125 aerosols. NaCl, one of the major components of marine aerosols, was selected as the inorganic component
126 since it was previously reported that organic acids contributed significantly to Cl depletion through a
127 reaction with NaCl (Laskin et al., 2012). In situ Raman analysis could clearly identify MBTCA and its
128 sodium salts during the hygroscopicity measurement despite NaCl being Raman inactive. To the best of
129 the authors' knowledge, this is the first study on the hygroscopic behavior and chemical reactivity of
130 MBTCA and its sodium salts thus far. The results are expected to promote more precise thermodynamic
131 models (Clegg et al., 2003). The phase transitions were observed by monitoring the size changes together
132 with the Raman spectra evolutions of the aerosol particles as a function of the RH. RMS can provide
133 information on chemical functional groups, water contents, molecular interactions, and phase states of the
134 aerosol particles. Such data can help understand the hygroscopic behavior of complex aerosol particles
135 better (Lee et al., 2008; Li et al., 2017; Wang et al., 2017). The molecular characterization of organic
136 aerosols can provide better insights into the potential mechanisms of SOA formation and transformation
137 (or aging) (Hallquist et al., 2009). Scanning electron microscopy (SEM)/energy-dispersive X-ray

spectroscopy (EDX) mapping was used to examine the elemental composition distribution in effloresced particles.

2. Experimental Section

2.1 Sample preparation

Pure 0.3 M solutions of NaCl (>99.9% purity, Sigma-Aldrich) and MBTCA (98%, Toronto Research Chemicals, TCR) were prepared. The mixture solutions of MBTCA and NaCl were prepared with molar mixing ratios of MBTCA:NaCl = 1:1, 1:2, 1:3, and 2:1. Mono-/di-/tri-sodium MBTCA salt solutions were obtained by mixing MBTCA and NaOH (>99.9% purity, Sigma-Aldrich) with molar ratios of MBTCA:NaOH = 1:1, 1:2, and 1:3, respectively. A mixture solution of MBTCA and monosodium MBTCA salt with a molar mixing ratio of 1:1 was prepared as well. All the solutions were made by dissolving the chemicals in the ultrapure de-ionized (DI) water (18 M Ω , Millipore Direct-QTM). Aerosol particles were generated by nebulizing the solutions using a single jet atomizer (HCT4810) on the Si wafer substrates (MTI Corporation, 99.999% purity). The size of the droplets examined at RH > 90% ranged from 1 to 15 μ m.

2.2 In situ Raman microspectrometry (RMS) for particles deposited on a Si wafer

During the hygroscopic measurements, in situ RMS was performed under a controlled RH to observe the hygroscopic behavior, structural changes, and chemical compositional variations of the aerosols generated from the solutions. The apparatus consisted of three parts: (A) see-through impactor, (B) Raman microscope/spectrometer, and (C) humidity-controlling system. The Si wafer substrate was mounted on the impaction plate in the see-through impactor. A more detailed discussion of the impactor and humidity-controlling system can be found elsewhere (Gupta et al., 2015). Briefly, the RH inside the impactor was controlled by mixing dry and wet (saturated with water vapor) N₂ (99.999% purity) gases. The flow rates of total 4 L·min⁻¹ of the dry and wet N₂ gases were controlled by two mass flow controllers to obtain the desired RH in the range of ~1–95%, which was monitored using a digital hygrometer (Testo 645). The digital hygrometer was calibrated using a dew-point hygrometer (M2 Plus-RH, GE) to provide RH readings with \pm 0.5% reproducibility. The Raman spectra and optical images of the aerosol particles were

recorded by LabSpec6 using a confocal Raman microspectrometer (XploRA, Horiba Jobin Yvon) equipped with a $\times 50$, 0.5 numerical aperture objective (Olympus). An excitation laser with a wavelength of 532 nm and 6 mW power was used, and the scattered Raman signals were detected at specific RHs during the hygroscopic measurements using an air-cooled multichannel charge-coupled device (CCD) detector. The data acquisition time for each measurement was 120 s. The spectral resolution was 1.8 cm^{-1} using 1800 gr/mm. The optical images were recorded continuously in RH = 1% steps with a size of 904×690 pixels during the first dehydration (by decreasing RH from ~ 95 to $\sim 1\%$), followed by the humidification (by increasing RH from ~ 1 to $\sim 95\%$) experiments using a top video camera assembled in the Raman instrument and processed using an image analysis software (Matrox, Inspector v9.0). Each humidity condition was sustained for at least 2 mins in order to provide an enough time for condensing or evaporating of water. The changes in particle size with the RH were monitored by measuring the particle 2-D area in the optical images to generate hygroscopic curves. These curves are represented by the area ratio (A/A_0) as a function of RH, where the 2-D projected aerosol area at a given RH (A) is divided by that at the end of the dehydration process (A_0) (Ahn et al., 2010). All hygroscopic experiments were conducted at room temperature ($T = 22 \pm 1^\circ\text{C}$). Aerosol particles generated from a pure NaCl aqueous solution to check the accuracy of the system showed typical hysteresis curves with deliquescence RH (DRH) = $75.5(\pm 0.5)\%$ and efflorescence RH (ERH) = $46.3\text{--}47.6\%$ as shown in Fig. S2, which are consistent with the theoretical and reported values.

2.3 SEM/EDX X-ray mapping of effloresced particles deposited on Si wafer

SEM/EDX X-ray mapping was performed for effloresced particles to determine the morphology and spatial distribution of the chemical elements after the hygroscopicity measurements of individual particles (Ahn et al., 2010; Gupta et al., 2015). The measurements were carried out using a Jeol JSM-6390 SEM equipped with an Oxford Link SATW ultrathin window EDX detector. The resolution of the detector was 133 eV for Mn $K\alpha$ X-rays. The X-ray spectra and elemental X-ray maps were recorded under the control of Oxford INCA Energy software. A 10 kV accelerating voltage and 0.7 nA beam current were used, and the typical measuring time for the elemental mapping was five minutes. An elemental quantification

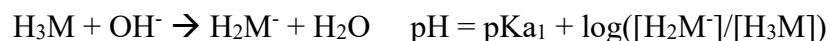
procedure, which is well described elsewhere (Wu et al., 2019a), was used for obtaining the elemental concentration.

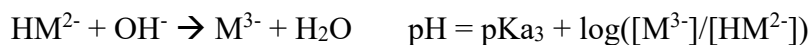
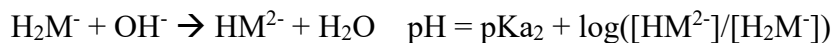
2.4 In situ RMS assembled with a levitation system

The levitation experimental set up consisted of coupling an acoustic (ultrasonic) levitator equipped with an environmental cell to an RMS, as shown in Fig. S1. The theory of acoustic levitation is described in detail elsewhere (Seaver et al., 1989). An ultrasonic levitator was modified (APOS BA 10, Tec5, Germany) to be installed within an environmental levitation cell consisting of two quartz windows, allowing the particle analysis (Seng et al., 2018). Two inlet/outlet valves were used for gas supplies to modify the relative humidity (RH) inside the cell. A sensor (SHT75 Sensirion) was placed in the cell to control the RH and temperature. The RH inside the chamber was controlled by mixing dry and wet Ar gases with a flow rate of 200 mL·min⁻¹ in the range of 10-80%(±1%) RH, and the temperature was T = 25±3 °C, making the experiments close to static flow conditions. The control of humidity and temperature allows limited droplet evaporation and long-term monitoring of the particles. The RMS measurements were performed with a LabRAM HR Evolution confocal spectrometer (Horiba Scientific, S.A) at certain RHs first during humidification and then during dehydration. The instrument was equipped with an ×50, 0.45 numerical aperture Olympus objective (WD = 13.8 mm) and a He-Ne laser (λ = 632.8 nm – 6 mW) with a theoretical lateral resolution of ~2 μm, and a depth of the laser focus corresponding to 16 μm with a Δz limit ≥ ±3 μm. The cell was mounted on an XYZ stage under the objective, allowing an adjustment of the droplet in the optimal position for the measurements. The mean size of the initial droplet injected in the levitator was 80 μm. The Raman spectra and optical images recorded at specific RHs were analyzed similarly to those obtained on the Si wafer.

2.5 Measurement of acid dissociation constants of MBTCA

MBTCA is a tri-carboxylic acid with three acid dissociation constants. To determine the three constants, a 0.02 M, 5 ml MBTCA solution was titrated with a 0.1 M NaOH solution, where the constants were determined based on the Henderson-Hasselbalch equations (Harris, 2012):





where H_3M , H_2M^- , HM^{2-} , and M^{3-} represent aqueous MBTCA, mono-, di-, and tri-sodium MBTCA anions, respectively. The $\text{pK}_{\text{a}1}$, $\text{pK}_{\text{a}2}$, and $\text{pK}_{\text{a}3}$ are the pHs when $[\text{H}_3\text{M}]$, $[\text{H}_2\text{M}^-]$, and $[\text{HM}^{2-}]$ equal $[\text{H}_2\text{M}^-]$, $[\text{HM}^{2-}]$, and $[\text{M}^{3-}]$, respectively, during the acid-base titration. Specifically, when NaOH was added at 0.5, 1.5, and 2.5 ml, the corresponding pHs of the solution are the three constants, which were 3.59, 4.85, and 6.79. Fig. 1 shows the calculated titration curve of MBTCA using the three determined K_a values, which is the same as the experimentally obtained titration data, supporting the validity of the K_a values, which were not reported so far.

3. Results and Discussion

3.1 Hygroscopic behavior of pure MBTCA particles

Wet-deposited MBTCA aerosols exhibited three types of hygroscopic behavior. As shown in Fig. 2, during the dehydration process, the exemplar droplets of types 1 and 2 shrank continuously with decreasing RH due to water evaporation until RHs = 58.4% and 40%, and then effloresced promptly at RH = 57.8% and gradually at RH = 39 - 35%, respectively. The effloresced particles maintained their size and shape with further decreases in RH. Whereas, the type 3 aerosols decreased continuously in size without a distinct change from RH = 94% to RH = 3% during the dehydration process. During the humidification process, types 1 and 2 particles kept the same size and shape until RH = ~90%, while type 3 particles experienced a gradual shrinkage at RH = 34-36.7% and remained the same until RH = ~85%. Fig. 2 also presents the corresponding optical images and in situ Raman spectra to assess the structural evolution of the MBTCA aerosols during the dehydration and humidification processes. Briefly, Raman peaks at ~1411 - 1420 cm^{-1} , ~1460 and ~2950 cm^{-1} , ~1660 - 1730 cm^{-1} , and ~3420 - 3475 cm^{-1} are for vibrations of C=O from COO^- , CH, C=O from COOH, and OH from water, respectively (Edsall, 1937; An et al., 2016). The redshift of the C=O peak (from COOH) from 1715 to 1660 cm^{-1} with decreasing FWHH (full width at half height), which is consistent with the standard MBTCA crystal, and the irregular shape and rough surface of types 1 and 2 aerosols at RH = 57.8% and 35%, respectively, confirmed that the particles effloresced into a solid phase. The optical images in the inset above the hygroscopic curve

of the type 2 particles showed gradual efflorescence at $RH = 39 - 35\%$. The water peak at $\sim 3475\text{ cm}^{-1}$ disappeared as well after the efflorescence. In contrast, type 3 aerosols maintained a circular morphology until $RH = 3\%$, as shown in the optical images in Fig. 2, even though an overlapped C=O (from COOH) peak at $1660 - 1680\text{ cm}^{-1}$ appeared during the dehydration process, and the water peak became undetectable, as shown in the Raman spectra at $RHs = 45\%$ and 3% , suggesting an amorphous/solid-state and the presence of an activation barrier or diffusional resistance to homogeneous nucleation required for the crystallization of MBTCA droplets as efflorescence is a kinetically controlled process (Martin, 2000; Freedman, 2017). Previous studies reported that α -pinene SOAs were very likely to exist as a highly viscous semisolid or even glassy state at low humidity (Saukko et al., 2012; Renbaum-Wolff et al., 2013; Berkemeier et al., 2014; Dette et al., 2014; Kidd et al., 2014; Song et al., 2016; Lessmeier et al., 2018). In addition, many organic substances, such as carboxylic acids, carbohydrates, and proteins, tend to form amorphous rather than crystalline phases upon the drying of aqueous solution droplets (Mikhailov et al., 2009). During the humidification process, the Raman spectra and morphology remained unchanged for types 1 and 2 particles until $RH = \sim 90\%$, where a slight decrease in morphology was observed due to structural re-arrangements by the absorption of moisture on the lattice imperfections (Gysel et al., 2002). Besides, the substrate can also affect this shrinkage. Especially, the hydrophilic substrate (such as Si wafer used in this study) seems to favor the phenomenon (Eom et al., 2014). Type 3 particles during the humidification process became irregular in shape, and the overlapped C=O (from COOH) peak shifted to 1660 cm^{-1} at $RH = 36.7\%$, as shown in the optical image and Raman spectrum, indicating the formation of solids. With the further increase in RH , particles maintained their size and shape until $RH = 85\%$, where they started to decrease in size due to a re-arrangement in structure. All types of MBTCA particles maintained the crystal phase until $RH = 95\%$.

Specifically, the types of pure MBTCA particles were classified as, “type 1: with a prompt efflorescence at $\sim 50\%$ RH during dehydration; type 2: with a gradual efflorescence at $\sim 35\%$ RH during dehydration; type 3: with a gradual efflorescence at $\sim 37\%$ RH during humidification”, based on their different behavior when efflorescence occurred. The different efflorescence behavior was attributed to different nucleation mechanisms: heterogeneous nucleation for types 1 and 2 particles (seed-containing), and homogeneous nucleation for type 3 particles (pure). MBTCA powders, which was used for making

the MBTCA solution, has intrinsic unknown impurity of 2%, and they were used without any purification. When MBTCA powders were dissolved in DI water and particles were generated by the nebulization of the aqueous solution using N₂ gas, impurities were either absent or associated with the droplets. The impurities existed in types 1 and 2 particles after nebulization, acting as seed crystals to induce efflorescence. Aqueous moieties in particles were reported to effloresce more easily by heterogeneous nucleation in the presence of seeds (Schlenker and Martin, 2005; Li et al., 2014; Gupta et al., 2015). The lower ERH and gradual efflorescence of type 2 compared to type 1 particles might be due to the less amount of impurities. Type 3 particles contain negligible or no seed crystals, and large kinetic barrier and/or diffusional resistance make the formation of the crystal structure difficult owing to the decreasing availability of condensed water during dehydration, so that they did not experience any efflorescence. A similar situation was observed for NH₄NO₃, NaNO₃, and NH₄HSO₄ particles (Lightstone et al., 2000; Hoffman et al., 2004; Gibson et al., 2006; Kim et al., 2012; Jing et al., 2018; Sun et al., 2018; Wu et al., 2019b). The Si substrates used in this study could also facilitate efflorescence (Eom et al., 2014; Wang et al., 2017). The efflorescence during humidification like type 3 particles was previously reported for Amazonian rain forest aerosols (Pöhlker et al., 2014) and the laboratory-generated NaCl–MgCl₂ mixture particles (Gupta et al., 2015). Thus, this phenomenon is not rare. And it was claimed that the aerosol particles initially had amorphous or poly-crystalline structures and underwent restructuring through kinetic water and ion mobilization in the presence of sufficient condensed water, resulting in overcoming the kinetic barrier and crystallization during humidification.

Among 100 particles, type 1-3 particles accounted for approximately 25%, 5%, and 70%, respectively, suggesting that MBTCA has slow homogeneous nucleation rate. Based on the experimental results, MBTCA droplets have DRH > 95% and ERH = 30–58%. This is the first study reporting the hygroscopic properties of MBTCA. A previous study showed that MBTCA was not hydrated significantly in the ambient atmosphere (Kildgaard et al., 2018), and our results also implied that the MBTCA solids stay in the air once they effloresced, based on our results.

3.2 Hygroscopic behavior of mono-/di-/tri-sodium MBTCA salt aerosols

304 The hygroscopicity and Raman spectra of mono-/di-/tri-sodium MBTCA salt aerosols (hereafter,
305 denoted as NaH_2M , Na_2HM , and Na_3M , respectively) were studied to examine the hygroscopic behavior
306 and estimate the chemical reactivity of MBTCA with NaCl . Figs. 3(a)-(c) show the 2-D projected area
307 ratio plot of aerosol particles generated from 0.3 M NaH_2M , Na_2HM , and Na_3M aqueous solutions as a
308 function of the RH together with the corresponding optical images and Raman spectra recorded at specific
309 RHs. As shown in Figs. 3(a) and (b), NaH_2M and Na_2HM aerosols shrank and grew continuously without
310 a phase transition during the dehydration and humidification processes, respectively, which is also
311 reflected in the optical images and Raman spectra, where they maintained their circular morphology only
312 with a change in size and the same Raman peak patterns and positions with small variations in the relative
313 peak intensities during the entire process. The water peak at $\sim 3400\text{--}3500\text{ cm}^{-1}$ can still be observed at the
314 end of the dehydration process. Even after being kept in a desiccator for two months, NaH_2M and Na_2HM
315 particles still showed the same shapes and Raman spectra with those at RHs = 3.4% and 2.8%,
316 respectively. These results indicate the non-crystallizable properties and supersaturated amorphous phase
317 state of the particles. The Na_3M particles behaved differently as they did not crystallize during the
318 dehydration process. On the other hand, the aerosols exhibited efflorescence at RH = 46.8% during the
319 humidification process (Fig. 3(c)), deliquesced to become a droplet at RH = 53.1%, and grew continuously
320 after that with increasing RH. The Raman spectra of the Na_3M particles in Fig. 3(c) showed that the peak
321 at $1420\text{--}1460\text{ cm}^{-1}$ became two sharp peaks when the particles effloresced, and the OH peak at 3400 cm^{-1}
322 indicates that Na_3M particles possibly exist in the hydrated form. The Na_3M particles behaved
323 analogously to type 3 MBTCA particles, which might be due to their similar structures when all three
324 COOH in MBTCA were replaced with COONa upon the reaction between MBTCA with NaOH. Since
325 all the observed Na_3M particles on the substrate (around 100 particles) behaved exactly in the same way
326 with crystallization during humidification process, the major contribution to the crystallization of Na_3M
327 particles is homogeneous crystallization, instead of heterogeneous crystallization induced by impurities
328 and Si substrate effect. Based on the top Raman spectra of aqueous MBTCA, NaH_2M , Na_2HM , and Na_3M
329 aerosols in Figs. 2 and 3, the ratios of the CH peak at $\sim 1460\text{ cm}^{-1}$ to the C=O peak at $\sim 1720\text{ cm}^{-1}$ (from
330 COOH) and to the C=O peak at $\sim 1420\text{ cm}^{-1}$ (from COO^-) increased and decreased in the order of MBTCA,

NaH₂M, Na₂HM, and Na₃M because of their reduced and elevated levels of COOH and COO⁻, respectively.

3.3 Hygroscopic behavior of MBTCA-NaCl mixture aerosols

Aerosols were generated by the nebulization of MBTCA-NaCl mixture solutions of molar mixing ratios of MBTCA:NaCl = 1:1, 1:2, 1:3, and 2:1 and deposited on Si wafer substrates, while maintaining the entire hygroscopic measurement system at RH > 90%. The hygroscopic behavior was investigated for ~10 individual aerosols of each mixing ratio, which are discussed in the following sections.

3.3.1 Aerosols generated from solutions of MBTCA:NaCl = 1:1 and 2:1

Fig. 4 presents the hygroscopic curves of representative aerosols nebulized from solutions of MBTCA:NaCl mixtures at different molar ratios (1:1 and 2:1) along with the corresponding optical images and Raman spectra at specific RHs. During the dehydration process, the circular liquid droplets decreased in size gradually without any noticeable phase change. The Raman peak patterns were maintained only with the C=O peak at 1721 cm⁻¹ (from COOH) shifting mildly rightwards, the water peak at 3466 cm⁻¹ becoming undetectable, and the relative peak intensities at ~1411, 1457, and 1721 cm⁻¹ varied when the RH was as low as 1.2%, indicating that the liquid droplets formed amorphous solids. The peak at 1680 cm⁻¹ on the Raman spectra of MBTCA:NaCl = 2:1 at RH = 1.2% suggested that the amorphous structure of the remaining MBTCA had been retained. Both MBTCA and NaCl have their DRHs and ERHs. Therefore, a step-wise efflorescence would happen if it is assumed that the mixture aerosols are an MBTCA-NaCl binary system, i.e., a component of the aqueous droplets precipitates first at their specific ERHs depending on their mixing ratios, and the second crystallization from the remnant eutonic solution occurs at their mutual ERH (MERH) with further decreases in RH, which is independent of the mixing ratios, generally forming a heterogeneous, core-shell crystal structure owing to the two-stage crystallization process (Ge et al., 1996; Gupta et al., 2015). However, the particles of MBTCA:NaCl = 1:1 and 2:1 mixing ratios did not follow the step-wise transitions in the present study, revealing that the aerosols do not belong to the MBTCA-NaCl binary system and the chemical compositions evolved during the hygroscopic experiment due to the reaction between MBTCA and NaCl, which will be discussed later.

During the humidification process, aerosol particles of two mixing ratios grew continuously when the RH was increased from 1.2% to 90% with C=O peak (from COOH) shifting back to $\sim 1721\text{ cm}^{-1}$ and the water peak becoming significant, as shown in Fig. 4. Several small crystal-like spots, which are marked by a dotted circle on the inset optical image beside the hygroscopic curve in Fig. 4(a), appeared in the particles with the mixing ratio of MBTCA:NaCl = 1:1 when the RH was increased to 67.2% and dissolved completely at RH = 71.2%. As the Raman spectra did not show any signals of the crystallized organics and RH = 71.2% is close to the DRH of pure NaCl ($75(\pm 0.5)\%$), the crystal-like moieties should result from the effloresced NaCl. The more noticeable water peak in the Raman spectrum taken at RH = 71.2% than that at RH = 67.2% also supports that the NaCl dissolved at RH = 71.2% as NaCl is quite hygroscopic (Li et al., 2017). No phase transition of NaCl was detected during the dehydration process, probably because the supersaturated organic moiety inhibited the crystallization of NaCl. The observation of effloresced particles during the humidification process might be caused by the structural re-arrangement of the amorphous particles upon the slow and continuous absorption of moisture with increasing RH (Mikhailov et al., 2009), leading to less restriction to NaCl crystallization. Indeed, organics in organic-inorganic mixture aerosols were reported to be a minor disturbance to the DRH of inorganic salts; in contrast, they may markedly decrease the ERH of inorganic salts depending on the organic type (Parsons et al., 2004).

3.3.2 Aerosols generated from solutions of MBTCA:NaCl = 1:2 and 1:3

Fig. 5 shows the hygroscopic curves of aerosol particles nebulized from solutions of MBTCA:NaCl with molar mixing ratios of 1:2 and 1:3, together with the corresponding optical images and Raman spectra at the transition RHs. During the dehydration process, droplets from the solutions of MBTCA:NaCl = 1:2 and 1:3 decreased gradually in size owing to water evaporation until a single-stage transition was observed at RHs = 47.2-46.5% and 46.7-45.8%, respectively, where the particle shape became less circular in the optical images. At this point, the following were observed in the Raman spectra: the water peak at 3455 cm^{-1} disappeared; the C=O peak at $\sim 1722/1720\text{ cm}^{-1}$ (from COOH) shifted slightly rightwards; the relative peak intensities at 1417/1416, 1461, and $1722/1720\text{ cm}^{-1}$ varied. With the further decreases in RH until $\sim 6\%$, the particles kept their size and shape. During the humidification process, all

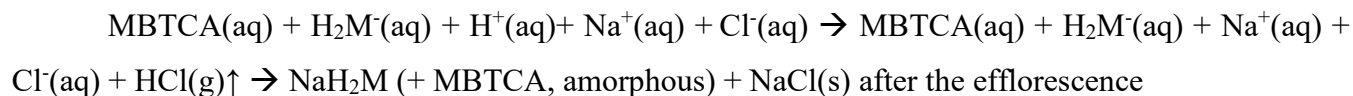
particles of MBTCA:NaCl = 1:2 and 1:3 maintained their structure until RHs = 50% and 40%, respectively, where they experienced a size decrease due to structural re-arrangement until RH = ~70%, grew continuously to become circular at RH = ~73%, and totally deliquesced into homogeneous droplets at RHs = 73.9% and 74.5%, respectively. Particle size and water peak increased rapidly, and the C=O peak (COOH) shifted back to 1720 cm⁻¹. Upon a further increase in RH, they grew continuously by water absorption. The ERH and DRH were attributed to the NaCl moiety as the Raman spectra maintained the peak patterns during the entire process, and the organic components condensed onto the NaCl crystal core almost simultaneously as an amorphous shell when efflorescence occurred, which is also indicated by the optical images. Before the complete deliquescence of the NaCl crystal core, the water peak at ~3455 cm⁻¹ in the Raman spectra and the optical images at RH = 72.4% and 73.8% of the particles from the MBTCA:NaCl = 1:2 and 1:3 solutions show that the organic shell was in the liquid phase, meaning that the mixture particles were in a solid-liquid equilibrium state (Sun et al., 2018). The Raman spectra shown in the figures were all obtained in the center of the particles. The Raman spectra were obtained both at the center and the edge of the particles for comparison during the measurement when the heterogeneity appeared during the hygroscopic measurements. The spectra from the center and the edge were different only in the intensity since NaCl is Raman inactive. As shown in the Fig. S3, the Raman spectra which were obtained from the center and the edge of an exemplar MBTCA:NaCl = 1:3 particle during the humidification process, match well after normalization to the CH peak at 1460 cm⁻¹.

All the particles from MBTCA:NaCl = 1:2 and 1:3 solutions showed hysteresis curves with ERHs in the range of 46.7-45.2% and 47.2-45.6%, respectively, and DRHs = 73.9(±0.3)% and 74.5(±0.3)%, respectively.

3.3.3 Chemical reactivity of aerosols generated from MBTCA–NaCl mixture solutions

The first Raman spectra of the aerosols generated from MBTCA-NaCl mixture solutions in Figs. 4 and 5 were obtained before the dehydration process, which are comparable to that of pure MBTCA droplet particle in Fig. 2 except for a much stronger free water peak at 3450-3470 cm⁻¹ due to the presence of a more hygroscopic NaCl moiety. This suggests that upon nebulization from the solutions, the mixture droplets were mostly the MBTCA-NaCl binary system. The Raman spectra obtained at the beginning of

the dehydration process and the end of the humidification process revealed increased and decreased ratios of the CH peak at $\sim 1460\text{ cm}^{-1}$ to the C=O peaks at $\sim 1720\text{ cm}^{-1}$ (from COOH) and $\sim 1412\text{ cm}^{-1}$ (from COO⁻), respectively, which implies that the reaction between MBTCA and NaCl occurred during the hygroscopic experiment, leading to the decreased and increased levels of the COOH and COO⁻ moieties, respectively. It is worth noticing that the dehydration and humidification curves of the MBTCA-NaCl mixtures did not overlap with each other mainly because of the different amounts of NaCl in the dehydration and humidification processes. As shown in the Fig. S2, NaCl is quite hygroscopic with around four times change in 2-D area after deliquescence, so the decreased amount of NaCl in the mixtures also lead to the smaller 2-D area when the MBTCA-NaCl mixture particles experienced hygroscopic growth during the humidification process, compared to those before dehydration. Fig. 6(a) presents the Raman spectra of particles generated from MBTCA:NaCl = 1:1, 1:2, and 1:3 solutions together with that of NaH₂M particles obtained at the end of humidification by normalizing to the CH peak at 1458 cm^{-1} . The C=O peak intensities at 1720 cm^{-1} (from COOH) and 1412 cm^{-1} (from COO⁻) of the particles generated from the mixture solutions were higher and lower, respectively, than those of the NaH₂M particle, suggesting that the aerosols generated from the MBTCA-NaCl solutions produced only NaH₂M as the reaction product between MBTCA and NaCl, regardless of the mixing ratios. The droplet particles after the humidification process were present as an MBTCA-NaCl-NaH₂M ternary system with varying compositions. As the first acid dissociation constant of MBTCA ($\text{pK}_{\text{a}1} = 3.59$) is more than 1 and 3 orders of magnitude larger than the second ($\text{pK}_{\text{a}2} = 4.85$) and third ($\text{pK}_{\text{a}3} = 6.79$), respectively, H₂M⁻ is more abundant than HM²⁻ and M³⁻. The chemical reaction between NaCl and MBTCA would occur in the aqueous phase as follows:



The NaH₂M particles may exist as amorphous particles, as described before in section 3.2. Raman spectra of standard aerosols generated from solutions of MBTCA:NaH₂M = 0:1, 1:1, and 1:0 were obtained at different RHs to estimate the chemical reactivity of the aerosol particles generated from the MBTCA-

NaCl mixture solutions, which were used as a calibration curve to help determine the relative MBTCA and NaH₂M contents in the aerosols at specific RHs. The estimation of the chemical reactivity between malonic acid and NaCl performed in the similar way was reported in a previous study (Li et al., 2017). The Raman spectra of MBTCA, NaH₂M, and mixture aerosols of MBTCA:NaH₂M = 1:1 obtained at RH = 90% and normalized to the CH₃ peak at 1460 cm⁻¹ showed that the intensity ratio of the two peaks at 1460 cm⁻¹ (CH₃) and ~1720 cm⁻¹ (C=O from COOH) (i.e., I₁₄₆₀/I₁₇₂₀) increased with increasing NaH₂M level because of the decreased COOH content, as shown in Fig. 6(b). The ratio, I₁₄₆₀/I₁₇₂₀, for each standard aerosol exhibited good linearity as a function of RH, as shown in Fig. 7(a), where the mean values obtained from 10 aerosols of each standard aerosol sample are plotted with error-bars. The Raman intensity ratios of the standard aerosols increased with decreasing RH because the C=O stretching vibrations of the free COOH group in the aqueous phase and the intramolecular hydrogen-bonded COOH group in the supersaturated phase become weaker and stronger (Bertran et al., 2010), respectively, with decreasing RH during the dehydration process.

The dependency of the I₁₄₆₀/I₁₇₂₀ ratios on RH can be used to estimate the MBTCA and NaH₂M (monosodium MBTCA salt) contents in the NaCl-MBTCA aerosols at specific RHs based on the calibration curve and to calculate the further reactivity. The chemical reactivity of the mixtures is represented as the degree of the reaction, which is defined as the ratio of consumed to the original amount of the limiting reactant. For example, for aerosols from solutions of MBTCA:NaCl = 2:1 and 1:2, NaCl and MBTCA are the limiting reactants, respectively. Fig. 7(b) shows the degree of the reaction of aerosols generated from solutions of each mixing ratio, where the mean degree of reaction has ~1.5-4% deviations owing to statistical variations in the Raman peak intensities caused by the baseline correction procedure and the uncertainties involved in the calibration measurements. The reactivity was estimated at five stages during one cycle hygroscopic experiment.

Stage I; At the beginning of the hygroscopic experiment, no reaction occurred for all the mixed droplets based on their Raman spectra, i.e., the degree of the reaction is 0.

470 *Stage 2*; As the RH decreased during the dehydration process, the reaction continued in the
471 aqueous aerosols until efflorescence of the droplets with mixing ratios of MBTCA:NaCl = 1:2 and
472 1:3 had occurred, and until the water content of the aerosols with mixing ratios of MBTCA:NaCl
473 = 1:1 and 2:1 became insignificant. The degrees of the reaction of aerosols with mixing ratios of
474 1:1, 1:2, and 1:3 were approximately 30%, whereas that of 2:1 approached 85%.

475
476 *Stage 3*; The reaction of aerosols generated from the solution of mixing ratio of MBTCA:NaCl =
477 2:1 was complete at the end of the dehydration process, indicating the total consumption of NaCl
478 and the formation of an MBTCA:NaH₂M = 1:1 mixture aerosol. The Raman spectra of the aerosols
479 with mixing ratios of MBTCA:NaCl = 1:1, 1:2, and 1:3 at the end of the dehydration process were
480 unsuitable for the reactivity estimation mostly due to their heterogeneous structure in the presence
481 of a NaCl core.

482
483 *Stages 4 and 5*; The reaction proceeded after deliquescence when the free H⁺ and Cl⁻ became
484 available again for aerosols with mixing ratios of MBTCA:NaCl = 1:1, 1:2, and 1:3, and a small
485 increase in the degree of reaction (~5%) was observed at the end of humidification for these
486 mixture droplets.

487
488 Most of the reactions occurred in the aqueous phase during the dehydration process with considerable
489 amounts of aqueous H⁺ from MBTCA and Cl⁻ from NaCl available for HCl liberation. During the entire
490 experiment, the reactivity followed the sequence of MBTCA:NaCl = 2:1 > 1:3 > 1:2 > 1:1, where the
491 reactivity appeared to be enhanced when either of the reactants is enriched. On the other hand, the reaction
492 was complete only when aqueous H⁺ was sufficiently available, i.e., the reaction depended mostly on the
493 triacid level. The real-time aerosol mixture components based on the reactivity estimation of each mixing
494 ratio at specific RHs are shown on the hygroscopic curves in Figs. 4 and 5.

495 The morphology and elemental distribution of effloresced MBTCA-NaCl particles were examined by
496 SEM/EDX. Figure 8(a) shows the secondary electron images (SEIs) of the exemplar particles of each
497 mixing ratio. The elemental X-ray maps for MBTCA:NaCl = 1:1 and 1:2 particles suggest that the NaCl

solid moiety (represented by Na and Cl X-ray maps) crystallized homogeneously at small spots inside the organic moiety. For MBTCA:NaCl = 1:3 particles with a significant amount of NaCl, the NaCl solid existed as a core surrounded by the organic moiety. The organic mixture of MBTCA and NaH₂M (represented by C and Na) condensed onto the NaCl core almost simultaneously when efflorescence occurred, while maintaining a relatively circular morphology, even after being inserted into the vacuum SEM chamber, which also indicates the low crystallization tendency of the organic moiety. The different shapes of organic shell-inorganic core structures depending on the organic mass fraction and RH are reported elsewhere (Karadima et al., 2019). The homogeneous structure of C and Na and the absence of Cl for particles with mixing ratios of MBTCA:NaCl = 2:1, as shown in the corresponding SEIs and X-ray spectrum in Figs. 8(a) and (b), confirmed that the reaction was complete at the end of the dehydration process. The reaction between MBTCA and NaCl and the changes in the microstructures after the reaction are expected to have some atmospheric implications since they may have enhanced ability to facilitate further heterogeneous reactions in the atmosphere because of their low crystallization property. Na (from both NaH₂M and NaCl) and Cl (from NaCl) levels were used to estimate the degrees of reaction for the MBTCA:NaCl = 1:1, 1:2, 1:3, and 2:1 systems, which were estimated to be ~25%, ~30%, ~37%, and 100%, respectively, with well matching to those from the Raman analysis by 5-8% differences.

3.4 Hygroscopic behavior of pure MBTCA and MBTCA–NaCl mixture particles in the levitation system

The data acquired from the levitation system for contactless experiments on particles of ~80 μm were used to compare with those obtained for aerosols on the Si wafer in the see-through impactor. The droplets were introduced into the levitator and dried rapidly at RH = ~10% within 15 minutes (first rapid dehydration, i.e., a quenching process), and humidified progressively to RH = 80%. Once RH = 80%, the particles were dehydrated gradually until RH = ~10% (second dehydration).

Two types of hygroscopic behavior of pure MBTCA particles were observed, corresponding closely to types 1 and 3 aerosol particles in the see-through impactor system, **due to heterogeneous crystallization induced by impurity seed crystals and homogeneous crystallization, respectively**, confirming that once

525 the MBTCA particles overcome the kinetic barrier and effloresce into solids, they no longer capture water
526 significantly. The ERH was ~49-54%. The Raman spectra and optical images are not shown separately.

527 The Raman spectra and optical images of particles composed of MBTCA:NaCl = 1:1, 1:2, and 1:3
528 mixing ratios are shown in Fig. 9. After the first rapid dehydration of the particles, the existence of peaks
529 at 1655 and 1720 cm^{-1} was observed for all the mixtures, and the relative intensity of the peak at ~1720
530 cm^{-1} increased with the increase of the NaCl content, suggesting the formation of the mixture of solid
531 MBTCA and amorphous moiety either from MBTCA or NaH_2M . During the humidification process, the
532 Raman peak at 1720 cm^{-1} and the particle size grew continuously with increasing RH. Transitions were
533 observed at RH = ~71%, ~74.5%, and ~75% for MBTCA:NaCl = 1:1, 1:2, and 1:3 mixture particles,
534 respectively, with the water peak at ~3500 cm^{-1} becoming significant for the three compositions. However,
535 the shrinkage of the particles before deliquescence was not captured for the levitated particles, as the
536 particles are too big (~80 μm in average) for the structural rearrangement to be observed, and the 2-D
537 optical images of the particles were used for plotting the hygroscopic curves even though the particles
538 were levitated, which might lead to some missing information on the 3-D level. The observed transition
539 points were attributed to the deliquescence of NaCl within the particle with the MBTCA moiety partially
540 remaining as a solid phase, and the elevated NaCl content strongly enhanced the ability of the particles to
541 uptake water. The peak related to the solid portion at 1655 cm^{-1} disappeared only for the MBTCA:NaCl
542 = 1:3 mixture particles at the end of humidification, suggesting that the particle had transformed
543 completely into a droplet. During the second dehydration process, the particles showed the entire release
544 of water, as illustrated by the disappearance of the peak at 3500 cm^{-1} at RH = ~50%, i.e., the ERH, for all
545 the mixtures while maintaining the peak patterns and positions until the lowest RH. The Raman spectra
546 recorded at the end of dehydration revealed both solid and amorphous phases for the MBTCA:NaCl = 1:1
547 and 1:2 mixtures due to the existence of the peaks at 1655 and 1720 cm^{-1} . In contrast, only the 1720 cm^{-1}
548 associated with the amorphous composition was observed for the MBTCA:NaCl = 1:3 mixture,
549 suggesting that the reaction between MBTCA and NaCl was facilitated extensively by the increased NaCl
550 concentration while absorbing sufficient moisture. The conspicuous DRHs and ERHs of all the mixtures
551 in the levitation system demonstrated a smaller degree of reaction between MBTCA and NaCl compared
552 to those obtained in the see-through impactor, which might be caused by the relatively closed atmosphere

in the levitator as the default settings of N₂ flow inside the see-through impactor cell and the levitation cell were 4 and 0.2 L·min⁻¹, respectively, i.e., less release of HCl. The larger size of the levitated particles could limit the release of HCl (Kerminen et al., 1997). In addition, the quenching process, i.e., the starting point of the hygroscopicity experiments, induced the solidification of MBTCA, and further, a slow reaction between MBTCA and NaCl.

4. Conclusions and atmospheric implication

The hygroscopic behavior, physical states, and chemical reactivity of pure MBTCA particles, mono-/di-/tri-sodium MBTCA salt particles, and MBTCA-NaCl particles of different mixing ratios were examined by in situ RMS assembled with a see-through impactor as the starting point with dehydration. The DRHs and ERHs of the laboratory-generated particles in the micrometer size range at room temperature were determined by monitoring the change in the particle area in the 2-D optical images and the corresponding Raman spectra at transition points with RH variation of ~1-95%. Pure MBTCA showed three types of hygroscopic behaviors in that types 1 and 2 particles effloresced suddenly and gradually, respectively, at ERH = 30-58% during the dehydration process, whereas type 3 particles crystallized during the humidification process at RH = ~37%, not during the dehydration process because of a kinetic barrier to nucleation with limited condensed water. Subsequently, all particles maintained their crystal structure until RH = 95%. The mono- and di-sodium MBTCA salt aerosols did not show a clear ERH and DRH during the dehydration and humidification processes, respectively. In contrast, the tri-sodium MBTCA showed ERH = ~44.4-46.8% (during humidification) and DRH = ~53.1%. The MBTCA-NaCl droplets with molar mixing ratios of MBTCA:NaCl = 1:1 and 2:1 showed no distinct DRH and ERH because of the partial and complete reactions with NaCl, respectively, whereas those with ratios of MBTCA:NaCl = 1:2 and 1:3 experienced single-stage efflorescence and deliquescence governed by the excess NaCl. Only monosodium MBTCA (NaH₂M) could be formed as a result of the reaction between NaCl and MBTCA regardless of the mixing ratios, mostly during the dehydration process within the timescale of one to two hours according to Raman analysis, indicating that the MBTCA-NaCl mixture systems are in an MBTCA-NaH₂M-NaCl ternary system except when NaCl has reacted completely in the mixture aerosols of MBTCA:NaCl = 2:1 ratio. The MBTCA-NaH₂M existed as amorphous solids, even

when the excess crystalline NaCl acted as a heterogeneous nucleation core, which was also confirmed by X-ray mapping. The reaction occurred more rapidly with a more elevated concentration of either MBTCA or NaCl, and the controlling factor for the reactivity of the mixtures depended mostly on the availability of H^+ dissociated from the MBTCA tricarboxylic acid. The hygroscopic experiments for pure MBTCA and MBTCA-NaCl mixture particles were also performed in a levitation system with the starting point from humidification after the quenching process and the RH variation of ~10 to 80%. The results acquired from the levitation system are consistent with those obtained from the see-through impactor, only with less reaction between MBTCA and NaCl resulting from the airtight atmosphere inside the levitator and the partial solidification of MBTCA after the quenching process. In addition, the elevated NaCl moiety can eventually transform the solidified MBTCA into droplets through reactions when absorbing adequate moisture.

These observations are expected to have important atmospheric implications in that they may help to better understand the complexity of real ambient SOA and inorganic mixture particles. In this study, the hygroscopicity of MBTCA was altered significantly when mixed with NaCl due to the reaction, so that they are more likely to contribute to further gas-particle interactions. The amorphous phase state may influence the uptake of gaseous photo-oxidants as well as the chemical transformation and aging of atmospheric aerosols (Mikhailov et al., 2009). The observed aqueous shell with the solid core upon the humidification of the mixture particles with mixing ratios of MBTCA:NaCl = 1:2 and 1:3 before the total dissolution of NaCl can scatter solar radiation more efficiently (Adachi et al., 2011; Sun et al., 2018). The aerosol liquid water can promote heterogeneous aqueous-phase chemical processes, resulting in the facile formation of secondary aerosols (Cheng et al., 2016; Li et al., 2019). Recently, heterogeneous reactions in aerosol water were reported to be a significant mechanism for haze formation in North China (Sun et al., 2018). Overall, the hygroscopic curve, Raman signatures, and X-ray maps of the effloresced particles provided clear features of the hygroscopic behavior and chemical reactivity of the MBTCA-NaCl mixture system covered in this study. These results are expected to provide insights into the physicochemical characteristics and atmospheric chemistry of highly oxidized SOAs mixed with inorganic particles.

Data availability. The data used in this study are available upon request; please contact Chul-Un Ro (curo@inha.ac.kr).

Author contributions. LW, CB, SS, and CR designed the experiment. LW, CB, and SS carried out the measurements and/or analyzed the data. LW, CB, SS, PF, EP, EV, YS and CR contributed discussion of the data. LW, SS, and CR drafted the paper.

Competing interests. The authors declare that they have no conflict of interest.

Acknowledgments. This study was supported by Basic Science Research Programs through the National Research Foundation of Korea (NRF) funded by the Ministry of Education, Science, and Technology (NRF-2018R1A2A1A05023254) and by the National Strategic Project-Fine particle of the National Research Foundation of Korea (NRF) funded by the Ministry of Science and ICT (MSIT), the Ministry of Environment (ME), and the Ministry of Health and Welfare (MOHW) (2017M3D8A1090654). Authors thank the Region Nouvelle Aquitaine for the financial support of the SPECAERO project. This work was performed through international and collaborative programs supported by PHC STAR n° 38815XE and visiting scholars program from IDEX of the University of Bordeaux.

References

- Adachi, K., Freney, E. J., and Buseck, P. R.: Shapes of internally mixed hygroscopic aerosol particles after deliquescence, and their effect on light scattering, *Geophysical Research Letters*, 38, n/a-n/a, 10.1029/2011gl047540, 2011.
- Ahn, K.-H., Kim, S.-M., Jung, H.-J., Lee, M.-J., Eom, H.-J., Maskey, S., and Ro, C.-U.: Combined use of optical and electron microscopic techniques for the measurement of hygroscopic property, chemical composition, and morphology of individual aerosol particles, *Analytical chemistry*, 82, 7999-8009, 2010.
- Aljawhary, D., Zhao, R., Lee, A. K., Wang, C., and Abbatt, J. P.: Kinetics, Mechanism, and Secondary Organic Aerosol Yield of Aqueous Phase Photo-oxidation of alpha-Pinene Oxidation Products, *J Phys Chem A*, 120, 1395-1407, 10.1021/acs.jpca.5b06237, 2016.

- An, P., Yuan, C.-Q., Liu, X.-H., Xiao, D.-B., and Luo, Z.-X.: Vibrational spectroscopic identification of isoprene, pinenes and their mixture, *Chinese Chemical Letters*, 27, 527-534, 10.1016/j.ccllet.2016.01.036, 2016.
- Bateman, A. P., Bertram, A. K., and Martin, S. T.: Hygroscopic influence on the semisolid-to-liquid transition of secondary organic materials, *J Phys Chem A*, 119, 4386-4395, 10.1021/jp508521c, 2015a.
- Bateman, A. P., Gong, Z., Liu, P., Sato, B., Cirino, G., Zhang, Y., Artaxo, P., Bertram, A. K., Manzi, A. O., Rizzo, L. V., Souza, R. A. F., Zaveri, R. A., and Martin, S. T.: Sub-micrometre particulate matter is primarily in liquid form over Amazon rainforest, *Nature Geoscience*, 9, 34-37, 10.1038/ngeo2599, 2015b.
- Berkemeier, T., Shiraiwa, M., Pöschl, U., and Koop, T.: Competition between water uptake and ice nucleation by glassy organic aerosol particles, *Atmospheric Chemistry and Physics*, 14, 12513-12531, 10.5194/acp-14-12513-2014, 2014.
- Bernard, F., Ciuraru, R., Boreave, A., and George, C.: Photosensitized Formation of Secondary Organic Aerosols above the Air/Water Interface, *Environ Sci Technol*, 50, 8678-8686, 10.1021/acs.est.6b03520, 2016.
- Bertran, O., Armelin, E., Estrany, F., Gomes, A., Torras, J., and Alemán, C.: Poly (2-thiophen-3-yl-malonic acid), a polythiophene with two carboxylic acids per repeating unit, *The Journal of Physical Chemistry B*, 114, 6281-6290, 2010.
- Cheng, Y., Zheng, G., Wei, C., Mu, Q., Zheng, B., Wang, Z., Gao, M., Zhang, Q., He, K., and Carmichael, G.: Reactive nitrogen chemistry in aerosol water as a source of sulfate during haze events in China, *Science Advances*, 2, e1601530, 2016.
- Chu, B., Wang, K., Takekawa, H., Li, J., Zhou, W., Jiang, J., Ma, Q., He, H., and Hao, J.: Hygroscopicity of particles generated from photooxidation of α -pinene under different oxidation conditions in the presence of sulfate seed aerosols, *Journal of Environmental Sciences*, 26, 129-139, 10.1016/s1001-0742(13)60402-7, 2014.
- Clegg, S. L., Seinfeld, J. H., and Edney, E. O.: Thermodynamic modelling of aqueous aerosols containing electrolytes and dissolved organic compounds. II. An extended Zdanovskii–Stokes–Robinson approach, *Journal of aerosol science*, 34, 667-690, 2003.
- Cui, T., Green, H. S., Selleck, P. W., Zhang, Z., O'Brien, R. E., Gold, A., Keywood, M., Kroll, J. H., and Surratt, J. D.: Chemical Characterization of Isoprene- and Monoterpene-Derived Secondary Organic Aerosol Tracers in Remote Marine Aerosols over a Quarter Century, *ACS Earth and Space Chemistry*, 3, 935-946, 10.1021/acsearthspacechem.9b00061, 2019.
- Detle, H. P., Qi, M., Schroder, D. C., Godt, A., and Koop, T.: Glass-forming properties of 3-methylbutane-1,2,3-tricarboxylic acid and its mixtures with water and pinonic acid, *J Phys Chem A*, 118, 7024-7033, 10.1021/jp505910w, 2014.
- Ding, X., Wang, X.-M., Gao, B., Fu, X.-X., He, Q.-F., Zhao, X.-Y., Yu, J.-Z., and Zheng, M.: Tracer-based estimation of secondary organic carbon in the Pearl River Delta, south China, *Journal of Geophysical Research: Atmospheres*, 117, n/a-n/a, 10.1029/2011jd016596, 2012.
- Donahue, N. M., Henry, K. M., Mentel, T. F., Kiendler-Scharr, A., Spindler, C., Bohn, B., Brauers, T., Dorn, H. P., Fuchs, H., Tillmann, R., Wahner, A., Saathoff, H., Naumann, K. H., Mohler, O., Leisner, T., Muller, L., Reinnig, M. C., Hoffmann, T., Salo, K., Hallquist, M., Frosch, M., Bilde,

- M., Tritscher, T., Barmet, P., Praplan, A. P., DeCarlo, P. F., Dommen, J., Prevot, A. S., and Baltensperger, U.: Aging of biogenic secondary organic aerosol via gas-phase OH radical reactions, *Proc Natl Acad Sci U S A*, 109, 13503-13508, 10.1073/pnas.1115186109, 2012.
- Dunne, E. M., Gordon, H., Kurten, A., Almeida, J., Duplissy, J., Williamson, C., Ortega, I. K., Pringle, K. J., Adamov, A., Baltensperger, U., Barmet, P., Benduhn, F., Bianchi, F., Breitenlechner, M., Clarke, A., Curtius, J., Dommen, J., Donahue, N. M., Ehrhart, S., Flagan, R. C., Franchin, A., Guida, R., Hakala, J., Hansel, A., Heinritzi, M., Jokinen, T., Kangasluoma, J., Kirkby, J., Kulmala, M., Kupc, A., Lawler, M. J., Lehtipalo, K., Makhmutov, V., Mann, G., Mathot, S., Merikanto, J., Miettinen, P., Nenes, A., Onnela, A., Rap, A., Reddington, C. L., Riccobono, F., Richards, N. A., Rissanen, M. P., Rondo, L., Sarnela, N., Schobesberger, S., Sengupta, K., Simon, M., Sipila, M., Smith, J. N., Stozkhov, Y., Tome, A., Trostl, J., Wagner, P. E., Wimmer, D., Winkler, P. M., Worsnop, D. R., and Carslaw, K. S.: Global atmospheric particle formation from CERN CLOUD measurements, *Science*, 354, 1119-1124, 10.1126/science.aaf2649, 2016.
- Edsall, J. T.: Raman Spectra of Amino Acids and Related Compounds IV. Ionization of Di- and Tricarboxylic Acids, *The Journal of Chemical Physics*, 5, 508-517, 10.1063/1.1750067, 1937.
- Enami, S., and Sakamoto, Y.: OH-Radical Oxidation of Surface-Active cis-Pinonic Acid at the Air-Water Interface, *J Phys Chem A*, 120, 3578-3587, 10.1021/acs.jpca.6b01261, 2016.
- Eom, H. J., Gupta, D., Li, X., Jung, H. J., Kim, H., and Ro, C. U.: Influence of collecting substrates on the characterization of hygroscopic properties of inorganic aerosol particles, *Anal Chem*, 86, 2648-2656, 10.1021/ac4042075, 2014.
- Freedman, M. A.: Phase separation in organic aerosol, *Chemical Society Reviews*, 46, 7694-7705, 2017.
- Fu, P., Kawamura, K., Chen, J., and Barrie, L. A.: Isoprene, monoterpene, and sesquiterpene oxidation products in the high Arctic aerosols during late winter to early summer, *Environmental Science & Technology*, 43, 4022-4028, 2009.
- Fu, P. Q., Kawamura, K., Cheng, Y. F., Hatakeyama, S., Takami, A., Li, H., and Wang, W.: Aircraft measurements of polar organic tracer compounds in tropospheric particles (PM_{2.5}) over central China, *Atmospheric Chemistry and Physics*, 14, 4185-4199, 10.5194/acp-14-4185-2014, 2014.
- Ge, Z., Wexler, A. S., and Johnston, M. V.: Multicomponent aerosol crystallization, *Journal of Colloid and Interface Science*, 183, 68-77, 1996.
- Gibson, E. R., Hudson, P. K., and Grassian, V. H.: Physicochemical properties of nitrate aerosols: Implications for the atmosphere, *The Journal of Physical Chemistry A*, 110, 11785-11799, 2006.
- Gómez-González, Y., Wang, W., Vermeylen, R., Chi, X., Neirynck, J., Janssens, I. A., Maenhaut, W., and Claeys, M.: Chemical characterisation of atmospheric aerosols during a 2007 summer field campaign at Brasschaat, Belgium: sources and source processes of biogenic secondary organic aerosol, *Atmospheric Chemistry and Physics*, 12, 125-138, 10.5194/acp-12-125-2012, 2012.
- Guenther, A., Hewitt, C. N., Erickson, D., Fall, R., Geron, C., Graedel, T., Harley, P., Klinger, L., Lerdau, M., and McKay, W.: A global model of natural volatile organic compound emissions, *Journal of Geophysical Research: Atmospheres*, 100, 8873-8892, 1995.
- Gupta, D., Eom, H. J., Cho, H. R., and Ro, C. U.: Hygroscopic behavior of NaCl–MgCl₂ mixture particles as nascent sea-spray aerosol surrogates and observation of efflorescence during

humidification, *Atmospheric Chemistry and Physics*, 15, 11273-11290, 10.5194/acp-15-11273-2015, 2015.

Gysel, M., Weingartner, E., and Baltensperger, U.: Hygroscopicity of aerosol particles at low temperatures. 2. Theoretical and experimental hygroscopic properties of laboratory generated aerosols, *Environmental science & technology*, 36, 63-68, 2002.

Hallquist, M., Wenger, J. C., Baltensperger, U., Rudich, Y., Simpson, D., Claeys, M., Dommen, J., Donahue, N., George, C., and Goldstein, A.: The formation, properties and impact of secondary organic aerosol: current and emerging issues, *Atmospheric chemistry and physics*, 9, 5155-5236, 2009.

Harris, D. C.: *Exploring chemical analysis*, Macmillan, 2012.

Haywood, J., and Boucher, O.: Estimates of the direct and indirect radiative forcing due to tropospheric aerosols: A review, *Reviews of geophysics*, 38, 513-543, 2000.

Hoffman, R. C., Laskin, A., and Finlayson-Pitts, B. J.: Sodium nitrate particles: physical and chemical properties during hydration and dehydration, and implications for aged sea salt aerosols, *Journal of Aerosol Science*, 35, 869-887, 10.1016/j.jaerosci.2004.02.003, 2004.

Holopainen, J. K., Kivimaenpää, M., and Nizkorodov, S. A.: Plant-derived Secondary Organic Material in the Air and Ecosystems, *Trends Plant Sci*, 22, 744-753, 10.1016/j.tplants.2017.07.004, 2017.

Hong, Z., Zhang, H., Zhang, Y., Xu, L., Liu, T., Xiao, H., Hong, Y., Chen, J., Li, M., Deng, J., Wu, X., Hu, B., and Chen, X.: Secondary organic aerosol of PM_{2.5} in a mountainous forest area in southeastern China: Molecular compositions and tracers implication, *Sci Total Environ*, 653, 496-503, 10.1016/j.scitotenv.2018.10.370, 2019.

Hu, D., Bian, Q., Li, T. W. Y., Lau, A. K. H., and Yu, J. Z.: Contributions of isoprene, monoterpenes, β -caryophyllene, and toluene to secondary organic aerosols in Hong Kong during the summer of 2006, *Journal of Geophysical Research*, 113, 10.1029/2008jd010437, 2008.

Hu, Q. H., Xie, Z. Q., Wang, X. M., Kang, H., He, Q. F., and Zhang, P.: Secondary organic aerosols over oceans via oxidation of isoprene and monoterpenes from Arctic to Antarctic, *Sci Rep*, 3, 2280, 10.1038/srep02280, 2013.

Jang, M., Czoschke, N. M., Lee, S., and Kamens, R. M.: Heterogeneous atmospheric aerosol production by acid-catalyzed particle-phase reactions, *Science*, 298, 814-817, 2002.

Jaoui, M., Kleindienst, T., Lewandowski, M., Offenberg, J., and Edney, E.: Identification and quantification of aerosol polar oxygenated compounds bearing carboxylic or hydroxyl groups. 2. Organic tracer compounds from monoterpenes, *Environmental science & technology*, 39, 5661-5673, 2005.

Jimenez, J. L., Canagaratna, M., Donahue, N., Prevot, A., Zhang, Q., Kroll, J. H., DeCarlo, P. F., Allan, J. D., Coe, H., and Ng, N.: Evolution of organic aerosols in the atmosphere, *science*, 326, 1525-1529, 2009.

Jing, B., Tong, S., Liu, Q., Li, K., Wang, W., Zhang, Y., and Ge, M.: Hygroscopic behavior of multicomponent organic aerosols and their internal mixtures with ammonium sulfate, *Atmospheric Chemistry and Physics*, 16, 4101-4118, 10.5194/acp-16-4101-2016, 2016.

Jing, B., Wang, Z., Tan, F., Guo, Y., Tong, S., Wang, W., Zhang, Y., and Ge, M.: Hygroscopic behavior of atmospheric aerosols containing nitrate salts and water-soluble organic acids, *Atmospheric Chemistry and Physics*, 18, 5115-5127, 10.5194/acp-18-5115-2018, 2018.

- Kammer, J., Perraudin, E., Flaud, P. M., Lamaud, E., Bonnefond, J. M., and Villenave, E.: Observation of nighttime new particle formation over the French Landes forest, *Sci Total Environ*, 621, 1084-1092, 10.1016/j.scitotenv.2017.10.118, 2018.
- Kang, M., Fu, P., Kawamura, K., Yang, F., Zhang, H., Zang, Z., Ren, H., Ren, L., Zhao, Y., Sun, Y., and Wang, Z.: Characterization of biogenic primary and secondary organic aerosols in the marine atmosphere over the East China Sea, *Atmospheric Chemistry and Physics*, 18, 13947-13967, 10.5194/acp-18-13947-2018, 2018.
- Karadima, K. S., Mavrantzas, V. G., and Pandis, S. N.: Insights into the morphology of multicomponent organic and inorganic aerosols from molecular dynamics simulations, *Atmospheric Chemistry and Physics*, 19, 5571-5587, 10.5194/acp-19-5571-2019, 2019.
- Kerminen, V.-M., Pakkanen, T. A., and Hillamo, R. E.: Interactions between inorganic trace gases and supermicrometer particles at a coastal site, *Atmospheric Environment*, 31, 2753-2765, 1997.
- Kidd, C., Perraud, V., Wingen, L. M., and Finlayson-Pitts, B. J.: Integrating phase and composition of secondary organic aerosol from the ozonolysis of α -pinene, *Proceedings of the National Academy of Sciences*, 111, 7552-7557, 2014.
- Kildgaard, J. V., Mikkelsen, K. V., Bilde, M., and Elm, J.: Hydration of Atmospheric Molecular Clusters II: Organic Acid-Water Clusters, *J Phys Chem A*, 122, 8549-8556, 10.1021/acs.jpca.8b07713, 2018.
- Kim, H., Lee, M.-J., Jung, H.-J., Eom, H.-J., Maskey, S., Ahn, K.-H., and Ro, C.-U.: Hygroscopic behavior of wet dispersed and dry deposited NaNO_3 particles, *Atmospheric Environment*, 60, 68-75, 10.1016/j.atmosenv.2012.06.011, 2012.
- Kim, H., Zhang, Q., and Heo, J.: Influence of intense secondary aerosol formation and long-range transport on aerosol chemistry and properties in the Seoul Metropolitan Area during spring time: results from KORUS-AQ, *Atmospheric Chemistry and Physics*, 18, 7149-7168, 10.5194/acp-18-7149-2018, 2018.
- Koop, T., Bookhold, J., Shiraiwa, M., and Pöschl, U.: Glass transition and phase state of organic compounds: dependency on molecular properties and implications for secondary organic aerosols in the atmosphere, *Physical Chemistry Chemical Physics*, 13, 19238-19255, 2011.
- Kostenidou, E., Karnezi, E., Kolodziejczyk, A., Szmigielski, R., and Pandis, S. N.: Physical and Chemical Properties of 3-Methyl-1,2,3-butanetricarboxylic Acid (MBTCA) Aerosol, *Environ Sci Technol*, 52, 1150-1155, 10.1021/acs.est.7b04348, 2018.
- Kourtchev, I., Copolovici, L., Claeys, M., and Maenhaut, W.: Characterization of atmospheric aerosols at a forested site in Central Europe, *Environmental science & technology*, 43, 4665-4671, 2009.
- Kroll, J. H., and Seinfeld, J. H.: Chemistry of secondary organic aerosol: Formation and evolution of low-volatility organics in the atmosphere, *Atmospheric Environment*, 42, 3593-3624, 2008.
- Kubátová, A., Vermeylen, R., Claeys, M., Cafmeyer, J., Maenhaut, W., Roberts, G., and Artaxo, P.: Carbonaceous aerosol characterization in the Amazon basin, Brazil: novel dicarboxylic acids and related compounds, *Atmospheric Environment*, 34, 5037-5051, 2000.
- Kubátová, A., Vermeylen, R., Claeys, M., Cafmeyer, J., and Maenhaut, W.: Organic compounds in urban aerosols from Gent, Belgium: Characterization, sources, and seasonal differences, *Journal of Geophysical Research: Atmospheres*, 107, ICC 5-1-ICC 5-12, 10.1029/2001jd000556, 2002.

- Lai, C., Liu, Y., Ma, J., Ma, Q., Chu, B., and He, H.: Heterogeneous Kinetics of cis-Pinonic Acid with Hydroxyl Radical under Different Environmental Conditions, *J Phys Chem A*, 119, 6583-6593, 10.1021/acs.jpca.5b01321, 2015.
- Laskin, A., Moffet, R. C., Gilles, M. K., Fast, J. D., Zaveri, R. A., Wang, B., Nigge, P., and Shutthanandan, J.: Tropospheric chemistry of internally mixed sea salt and organic particles: Surprising reactivity of NaCl with weak organic acids, *Journal of Geophysical Research: Atmospheres*, 117, n/a-n/a, 10.1029/2012jd017743, 2012.
- Lee, A. K. Y., Ling, T. Y., and Chan, C. K.: Understanding hygroscopic growth and phase transformation of aerosols using single particle Raman spectroscopy in an electrodynamic balance, *Faraday Discuss.*, 137, 245-263, 10.1039/b704580h, 2008.
- Lessmeier, J., Dette, H. P., Godt, A., and Koop, T.: Physical state of 2-methylbutane-1,2,3,4-tetraol in pure and internally mixed aerosols, *Atmospheric Chemistry and Physics*, 18, 15841-15857, 10.5194/acp-18-15841-2018, 2018.
- Li, J. J., Wang, G. H., Cao, J. J., Wang, X. M., and Zhang, R. J.: Observation of biogenic secondary organic aerosols in the atmosphere of a mountain site in central China: temperature and relative humidity effects, *Atmospheric Chemistry and Physics*, 13, 11535-11549, 10.5194/acp-13-11535-2013, 2013.
- Li, X., Gupta, D., Eom, H.-J., Kim, H., and Ro, C.-U.: Deliquescence and efflorescence behavior of individual NaCl and KCl mixture aerosol particles, *Atmospheric Environment*, 82, 36-43, 10.1016/j.atmosenv.2013.10.011, 2014.
- Li, X., Gupta, D., Lee, J., Park, G., and Ro, C. U.: Real-Time Investigation of Chemical Compositions and Hygroscopic Properties of Aerosols Generated from NaCl and Malonic Acid Mixture Solutions Using in Situ Raman Microspectrometry, *Environ Sci Technol*, 51, 263-270, 10.1021/acs.est.6b04356, 2017.
- Li, X., Song, S., Zhou, W., Hao, J., Worsnop, D. R., and Jiang, J.: Interactions between aerosol organic components and liquid water content during haze episodes in Beijing, *Atmospheric Chemistry and Physics*, 19, 12163-12174, 10.5194/acp-19-12163-2019, 2019.
- Lightstone, J. M., Onasch, T. B., Imre, D., and Oatis, S.: Deliquescence, efflorescence, and water activity in ammonium nitrate and mixed ammonium nitrate/succinic acid microparticles, *The Journal of Physical Chemistry A*, 104, 9337-9346, 2000.
- Lignell, H., Epstein, S. A., Marvin, M. R., Shemesh, D., Gerber, B., and Nizkorodov, S.: Experimental and theoretical study of aqueous cis-pinonic acid photolysis, *J Phys Chem A*, 117, 12930-12945, 10.1021/jp4093018, 2013.
- Liu, T., Zhou, L., Liu, Q., Lee, B. P., Yao, D., Lu, H., Lyu, X., Guo, H., and Chan, C. K.: Secondary Organic Aerosol Formation from Urban Roadside Air in Hong Kong, *Environ Sci Technol*, 53, 3001-3009, 10.1021/acs.est.8b06587, 2019.
- Ma, Q., Ma, J., Liu, C., Lai, C., and He, H.: Laboratory study on the hygroscopic behavior of external and internal C2-C4 dicarboxylic acid-NaCl mixtures, *Environ Sci Technol*, 47, 10381-10388, 10.1021/es4023267, 2013.
- Marsh, A., Rovelli, G., Miles, R. E. H., and Reid, J. P.: Complexity of Measuring and Representing the Hygroscopicity of Mixed Component Aerosol, *J Phys Chem A*, 123, 1648-1660, 10.1021/acs.jpca.8b11623, 2019.

- Martin, S. T.: Phase transitions of aqueous atmospheric particles, *Chemical Reviews*, 100, 3403-3454, 2000.
- Mikhailov, E., Vlasenko, S., Martin, S., Koop, T., and Pöschl, U.: Amorphous and crystalline aerosol particles interacting with water vapor: conceptual framework and experimental evidence for restructuring, phase transitions and kinetic limitations, *Atmospheric Chemistry and Physics*, 9, 9491-9522, 2009.
- Miyazaki, Y., Jung, J., Fu, P., Mizoguchi, Y., Yamanoi, K., and Kawamura, K.: Evidence of formation of submicrometer water-soluble organic aerosols at a deciduous forest site in northern Japan in summer, *Journal of Geophysical Research: Atmospheres*, 117, n/a-n/a, 10.1029/2012jd018250, 2012.
- Müller, L., Reinnig, M. C., Naumann, K. H., Saathoff, H., Mentel, T. F., Donahue, N. M., and Hoffmann, T.: Formation of 3-methyl-1,2,3-butanetricarboxylic acid via gas phase oxidation of pinonic acid – a mass spectrometric study of SOA aging, *Atmospheric Chemistry and Physics*, 12, 1483-1496, 10.5194/acp-12-1483-2012, 2012.
- Mutzel, A., Rodigast, M., Iinuma, Y., Böge, O., and Herrmann, H.: Monoterpene SOA–contribution of first-generation oxidation products to formation and chemical composition, *Atmospheric environment*, 130, 136-144, 2016.
- Pajunoja, A., Hu, W., Leong, Y. J., Taylor, N. F., Miettinen, P., Palm, B. B., Mikkonen, S., Collins, D. R., Jimenez, J. L., and Virtanen, A.: Phase state of ambient aerosol linked with water uptake and chemical aging in the southeastern US, *Atmospheric Chemistry and Physics*, 16, 11163-11176, 2016.
- Parsons, M. T., Knopf, D. A., and Bertram, A. K.: Deliquescence and Crystallization of Ammonium Sulfate Particles Internally Mixed with Water-Soluble Organic Compounds, *The Journal of Physical Chemistry A*, 108, 11600-11608, 10.1021/jp0462862, 2004.
- Pöhlker, C., Saturno, J., Krüger, M. L., Förster, J.-D., Weigand, M., Wiedemann, K. T., Bechtel, M., Artaxo, P., and Andreae, M. O.: Efflorescence upon humidification? X-ray microspectroscopic in situ observation of changes in aerosol microstructure and phase state upon hydration, *Geophysical Research Letters*, 41, 3681-3689, 10.1002/2014gl059409, 2014.
- Poschl, U., and Shiraiwa, M.: Multiphase chemistry at the atmosphere-biosphere interface influencing climate and public health in the anthropocene, *Chem Rev*, 115, 4440-4475, 10.1021/cr500487s, 2015.
- Praplan, A. P., Barmet, P., Dommen, J., and Baltensperger, U.: Cyclobutyl methyl ketone as a model compound for pinonic acid to elucidate oxidation mechanisms, *Atmospheric Chemistry and Physics*, 12, 10749-10758, 10.5194/acp-12-10749-2012, 2012.
- Reid, J. P., Bertram, A. K., Topping, D. O., Laskin, A., Martin, S. T., Petters, M. D., Pope, F. D., and Rovelli, G.: The viscosity of atmospherically relevant organic particles, *Nat Commun*, 9, 956, 10.1038/s41467-018-03027-z, 2018.
- Renbaum-Wolff, L., Grayson, J. W., Bateman, A. P., Kuwata, M., Sellier, M., Murray, B. J., Shilling, J. E., Martin, S. T., and Bertram, A. K.: Viscosity of alpha-pinene secondary organic material and implications for particle growth and reactivity, *Proc Natl Acad Sci U S A*, 110, 8014-8019, 10.1073/pnas.1219548110, 2013.

- Rudich, Y., Donahue, N. M., and Mentel, T. F.: Aging of organic aerosol: Bridging the gap between laboratory and field studies, *Annual Review of Physical Chemistry*, 58, 321-352, 10.1146/annurev.physchem.58.032806.104432, 2007.
- Sato, K., Jia, T., Tanabe, K., Morino, Y., Kajii, Y., and Imamura, T.: Terpenylic acid and nine-carbon multifunctional compounds formed during the aging of β -pinene ozonolysis secondary organic aerosol, *Atmospheric Environment*, 130, 127-135, 10.1016/j.atmosenv.2015.08.047, 2016.
- Saukko, E., Lambe, A. T., Massoli, P., Koop, T., Wright, J. P., Croasdale, D. R., Pedernera, D. A., Onasch, T. B., Laaksonen, A., Davidovits, P., Worsnop, D. R., and Virtanen, A.: Humidity-dependent phase state of SOA particles from biogenic and anthropogenic precursors, *Atmospheric Chemistry and Physics*, 12, 7517-7529, 10.5194/acp-12-7517-2012, 2012.
- Schlenker, J. C., and Martin, S. T.: Crystallization pathways of sulfate–nitrate–ammonium aerosol particles, *The Journal of Physical Chemistry A*, 109, 9980-9985, 2005.
- Seaver, M., Galloway, A., and Manuccia, T. J.: Acoustic levitation in a free-jet wind tunnel, *Review of Scientific Instruments*, 60, 3452-3459, 10.1063/1.1140492, 1989.
- Seng, S., Guo, F., Tobon, Y. A., Ishikawa, T., Moreau, M., Ishizaka, S., and Sobanska, S.: Deliquescence behavior of photo-irradiated single NaNO_3 droplets, *Atmospheric Environment*, 183, 33-39, 10.1016/j.atmosenv.2018.04.007, 2018.
- Shiraiwa, M., Li, Y., Tsimpidi, A. P., Karydis, V. A., Berkemeier, T., Pandis, S. N., Lelieveld, J., Koop, T., and Poschl, U.: Global distribution of particle phase state in atmospheric secondary organic aerosols, *Nat Commun*, 8, 15002, 10.1038/ncomms15002, 2017.
- Shrivastava, M., Easter, R. C., Liu, X., Zelenyuk, A., Singh, B., Zhang, K., Ma, P.-L., Chand, D., Ghan, S., Jimenez, J. L., Zhang, Q., Fast, J., Rasch, P. J., and Tiitta, P.: Global transformation and fate of SOA: Implications of low-volatility SOA and gas-phase fragmentation reactions, *Journal of Geophysical Research: Atmospheres*, 120, 4169-4195, 10.1002/2014jd022563, 2015.
- Shrivastava, M., Cappa, C. D., Fan, J., Goldstein, A. H., Guenther, A. B., Jimenez, J. L., Kuang, C., Laskin, A., Martin, S. T., Ng, N. L., Petaja, T., Pierce, J. R., Rasch, P. J., Roldin, P., Seinfeld, J. H., Shilling, J., Smith, J. N., Thornton, J. A., Volkamer, R., Wang, J., Worsnop, D. R., Zaveri, R. A., Zelenyuk, A., and Zhang, Q.: Recent advances in understanding secondary organic aerosol: Implications for global climate forcing, *Reviews of Geophysics*, 55, 509-559, 10.1002/2016rg000540, 2017.
- Slade, J. H., Ault, A. P., Bui, A. T., Ditto, J. C., Lei, Z., Bondy, A. L., Olson, N. E., Cook, R. D., Desrochers, S. J., Harvey, R. M., Erickson, M. H., Wallace, H. W., Alvarez, S. L., Flynn, J. H., Boor, B. E., Petrucci, G. A., Gentner, D. R., Griffin, R. J., and Shepson, P. B.: Bouncer Particles at Night: Biogenic Secondary Organic Aerosol Chemistry and Sulfate Drive Diel Variations in the Aerosol Phase in a Mixed Forest, *Environ Sci Technol*, 53, 4977-4987, 10.1021/acs.est.8b07319, 2019.
- Song, M., Maclean, A. M., Huang, Y., Smith, N. R., Blair, S. L., Laskin, J., Laskin, A., DeRieux, W.-S. W., Li, Y., Shiraiwa, M., Nizkorodov, S. A., and Bertram, A. K.: Liquid–liquid phase separation and viscosity within secondary organic aerosol generated from diesel fuel vapors, *Atmospheric Chemistry and Physics*, 19, 12515-12529, 10.5194/acp-19-12515-2019, 2019.

- Song, Y. C., Haddrell, A. E., Bzdek, B. R., Reid, J. P., Bannan, T., Topping, D. O., Percival, C., and Cai, C.: Measurements and predictions of binary component aerosol particle viscosity, *The Journal of Physical Chemistry A*, 120, 8123-8137, 2016.
- Srivastava, D., Favez, O., Perraudin, E., Villenave, E., and Albinet, A.: Comparison of Measurement-Based Methodologies to Apportion Secondary Organic Carbon (SOC) in PM_{2.5}: A Review of Recent Studies, *Atmosphere*, 9, 10.3390/atmos9110452, 2018.
- Sun, J., Liu, L., Xu, L., Wang, Y., Wu, Z., Hu, M., Shi, Z., Li, Y., Zhang, X., Chen, J., and Li, W.: Key Role of Nitrate in Phase Transitions of Urban Particles: Implications of Important Reactive Surfaces for Secondary Aerosol Formation, *Journal of Geophysical Research: Atmospheres*, 123, 1234-1243, 10.1002/2017jd027264, 2018.
- Szmigielski, R., Surratt, J. D., Gómez-González, Y., Van der Veken, P., Kourtchev, I., Vermeylen, R., Blockhuys, F., Jaoui, M., Kleindienst, T. E., Lewandowski, M., Offenberg, J. H., Edney, E. O., Seinfeld, J. H., Maenhaut, W., and Claeys, M.: 3-methyl-1,2,3-butanetricarboxylic acid: An atmospheric tracer for terpene secondary organic aerosol, *Geophysical Research Letters*, 34, 10.1029/2007gl031338, 2007.
- Tang, M., Chan, C. K., Li, Y. J., Su, H., Ma, Q., Wu, Z., Zhang, G., Wang, Z., Ge, M., Hu, M., He, H., and Wang, X.: A review of experimental techniques for aerosol hygroscopicity studies, *Atmospheric Chemistry and Physics*, 19, 12631-12686, 10.5194/acp-19-12631-2019, 2019.
- Topping, D., Connolly, P., and McFiggans, G.: Cloud droplet number enhanced by co-condensation of organic vapours, *Nature Geoscience*, 6, 443, 2013.
- Virtanen, A., Joutsensaari, J., Koop, T., Kannosto, J., Yli-Pirilä, P., Leskinen, J., Mäkelä, J. M., Holopainen, J. K., Pöschl, U., and Kulmala, M.: An amorphous solid state of biogenic secondary organic aerosol particles, *Nature*, 467, 824, 2010.
- Vlachou, A., Tobler, A., Lamkaddam, H., Canonaco, F., Daellenbach, K. R., Jaffrezo, J.-L., Minguillón, M. C., Maasikmets, M., Teinmaa, E., Baltensperger, U., El Haddad, I., and Prévôt, A. S. H.: Development of a versatile source apportionment analysis based on positive matrix factorization: a case study of the seasonal variation of organic aerosol sources in Estonia, *Atmospheric Chemistry and Physics*, 19, 7279-7295, 10.5194/acp-19-7279-2019, 2019.
- Vogel, A. L., Äijälä, M., Corrigan, A. L., Junninen, H., Ehn, M., Petäjä, T., Worsnop, D. R., Kulmala, M., Russell, L. M., Williams, J., and Hoffmann, T.: In situ submicron organic aerosol characterization at a boreal forest research station during HUMPPA-COPEC 2010 using soft and hard ionization mass spectrometry, *Atmospheric Chemistry and Physics*, 13, 10933-10950, 10.5194/acp-13-10933-2013, 2013.
- Wang, B., O'Brien, R. E., Kelly, S. T., Shilling, J. E., Moffet, R. C., Gilles, M. K., and Laskin, A.: Reactivity of liquid and semisolid secondary organic carbon with chloride and nitrate in atmospheric aerosols, *J Phys Chem A*, 119, 4498-4508, 10.1021/jp510336q, 2015.
- Wang, X., Jing, B., Tan, F., Ma, J., Zhang, Y., and Ge, M.: Hygroscopic behavior and chemical composition evolution of internally mixed aerosols composed of oxalic acid and ammonium sulfate, *Atmospheric Chemistry and Physics*, 17, 12797-12812, 10.5194/acp-17-12797-2017, 2017.

- Wang, Z., Jing, B., Shi, X., Tong, S., Wang, W., and Ge, M.: Importance of water-soluble organic acid on the hygroscopicity of nitrate, *Atmospheric Environment*, 190, 65-73, 10.1016/j.atmosenv.2018.07.010, 2018.
- Wu, L., Li, X., Kim, H., Geng, H., Godoi, R. H. M., Barbosa, C. G. G., Godoi, A. F. L., Yamamoto, C. I., de Souza, R. A. F., Pöhlker, C., Andreae, M. O., and Ro, C.-U.: Single-particle characterization of aerosols collected at a remote site in the Amazonian rainforest and an urban site in Manaus, Brazil, *Atmospheric Chemistry and Physics*, 19, 1221-1240, 10.5194/acp-19-1221-2019, 2019a.
- Wu, L., Li, X., and Ro, C.-U.: Hygroscopic Behavior of Ammonium Sulfate, Ammonium Nitrate, and their Mixture Particles, *Asian Journal of Atmospheric Environment*, 13, 196-211, 10.5572/ajae.2019.13.3.196, 2019b.
- Wu, Z. J., Nowak, A., Poulain, L., Herrmann, H., and Wiedensohler, A.: Hygroscopic behavior of atmospherically relevant water-soluble carboxylic salts and their influence on the water uptake of ammonium sulfate, *Atmospheric Chemistry and Physics*, 11, 12617-12626, 10.5194/acp-11-12617-2011, 2011.
- Yasmeen, F., Szmigielski, R., Vermeylen, R., Gomez-Gonzalez, Y., Surratt, J. D., Chan, A. W., Seinfeld, J. H., Maenhaut, W., and Claeys, M.: Mass spectrometric characterization of isomeric terpenoic acids from the oxidation of alpha-pinene, beta-pinene, d-limonene, and Delta3-carene in fine forest aerosol, *J Mass Spectrom*, 46, 425-442, 10.1002/jms.1911, 2011.
- Yatavelli, R. L. N., Mohr, C., Stark, H., Day, D. A., Thompson, S. L., Lopez-Hilfiker, F. D., Campuzano-Jost, P., Palm, B. B., Vogel, A. L., Hoffmann, T., Heikkinen, L., Äijälä, M., Ng, N. L., Kimmel, J. R., Canagaratna, M. R., Ehn, M., Junninen, H., Cubison, M. J., Petäjä, T., Kulmala, M., Jayne, J. T., Worsnop, D. R., and Jimenez, J. L.: Estimating the contribution of organic acids to northern hemispheric continental organic aerosol, *Geophysical Research Letters*, 42, 6084-6090, 10.1002/2015gl064650, 2015.
- Zhang, Y. Y., Müller, L., Winterhalter, R., Moortgat, G. K., Hoffmann, T., and Pöschl, U.: Seasonal cycle and temperature dependence of pinene oxidation products, dicarboxylic acids and nitrophenols in fine and coarse air particulate matter, *Atmospheric Chemistry and Physics*, 10, 7859-7873, 10.5194/acp-10-7859-2010, 2010.

Figure 1. Calculated titration curve for MBTCA, noted as H_3M in this figure. The experimental data are shown as orange triangles. 5 mL of 0.02 M H_3M was titrated with a 0.1 M NaOH solution.

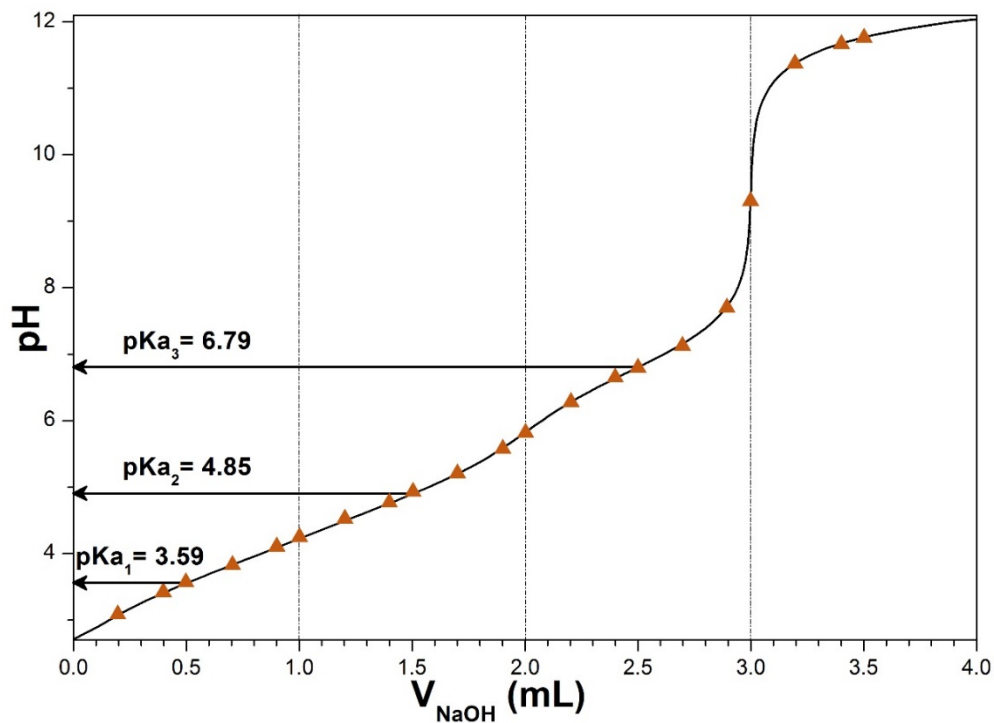
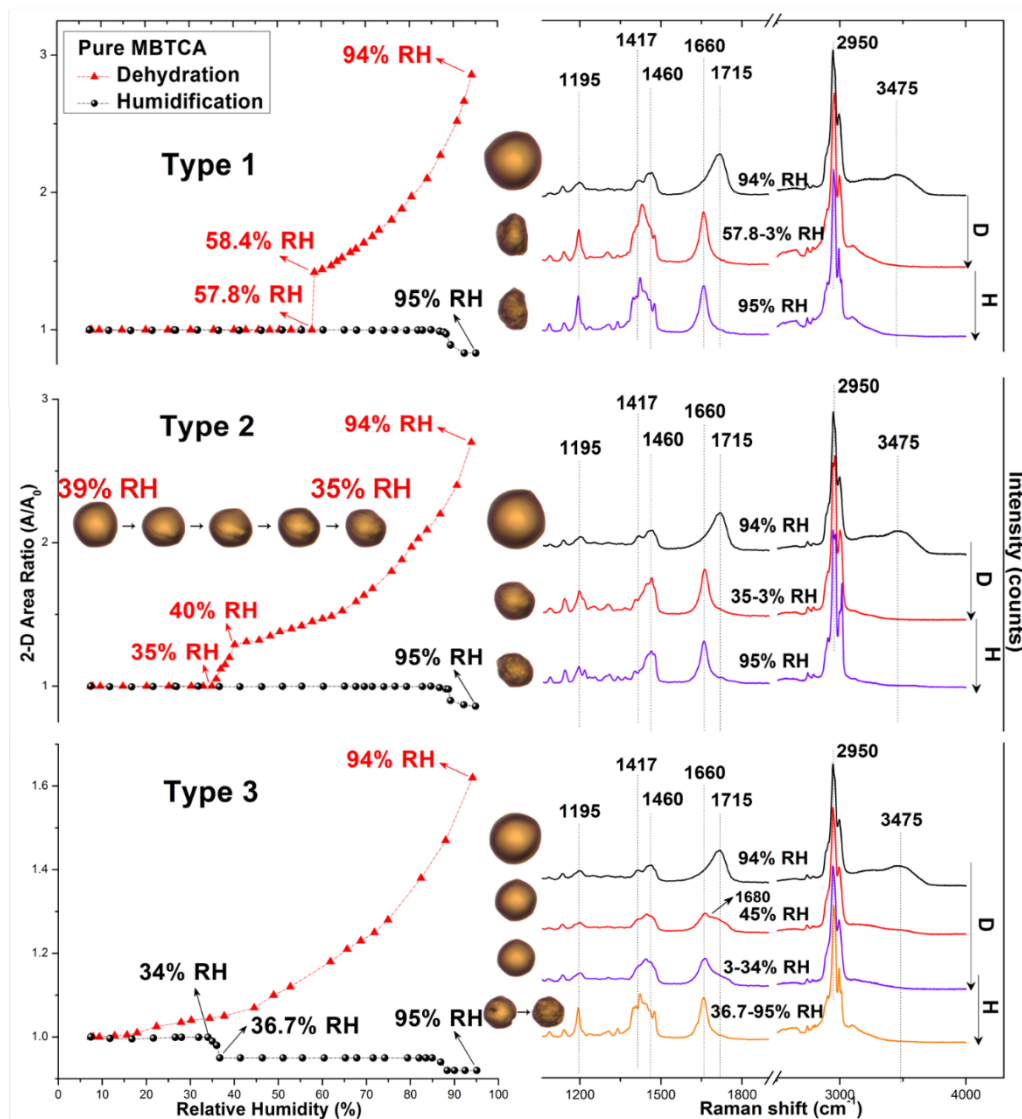
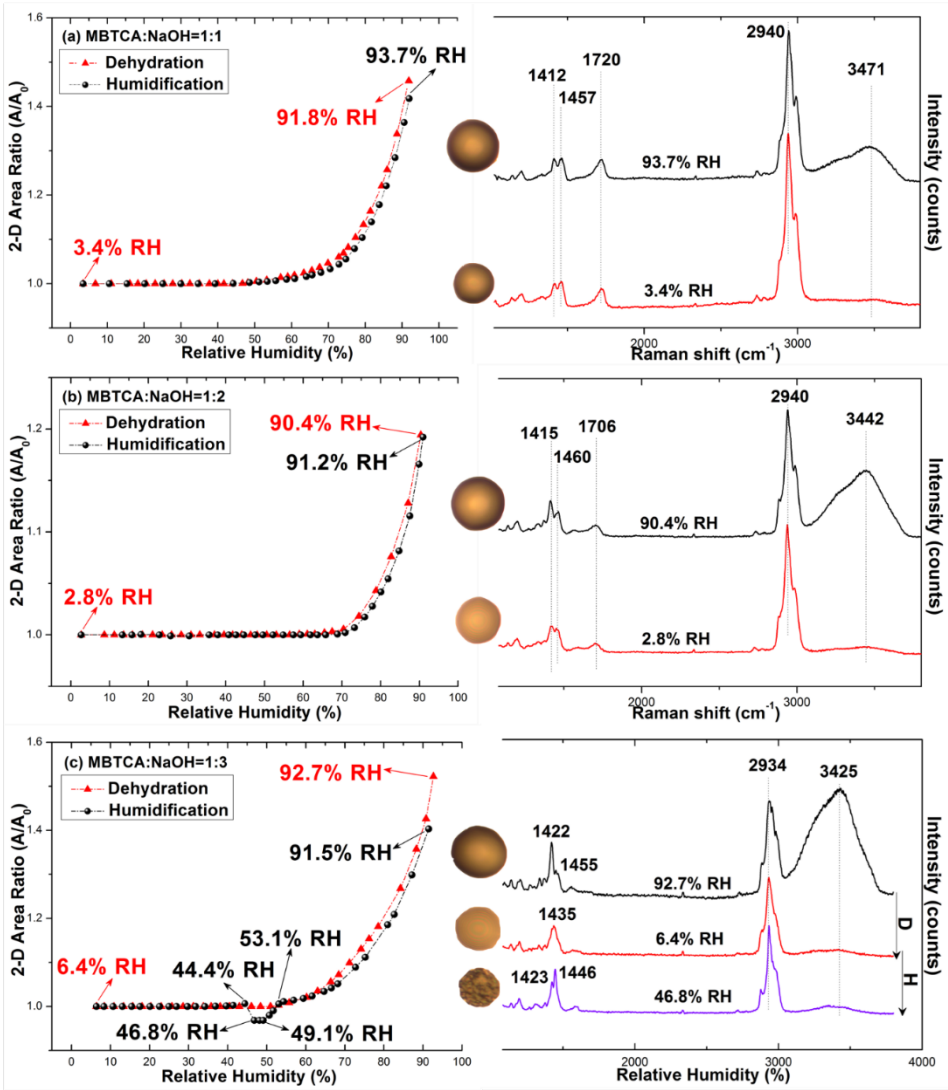


Figure 2. Hygroscopic curves, corresponding optical images, and Raman spectra at specific RHs of three types of pure MBTCA particles. The transition RHs recorded during the dehydration (D) and humidification (H) processes are marked with arrows in the hygroscopic curves.



1016
1017
1018
1019
1020

Figure 3. Hygroscopic curves, corresponding optical images, and Raman spectra at specific RHs of (a) mono-, (b) di-, and (c) tri-sodium MBTCA salt aerosols. The recorded transition RHs during the dehydration and humidification processes are marked with arrows in the hygroscopic curves.



1021 Figure 4. Hygroscopic curves, corresponding optical images, and Raman spectra at specific RHs of MBTCA:NaCl = (a) 1:1 and (b) 2:1.
 1022 The recorded transition RHs during the dehydration (D) and humidification (H) processes and the chemical compositions of the mixtures
 1023 at certain RHs are marked with arrows in the hygroscopic curves. The phase notations shown in parenthesis are s=solid; aq=aqueous;
 1024 and as=amorphous solid.
 1025
 1026

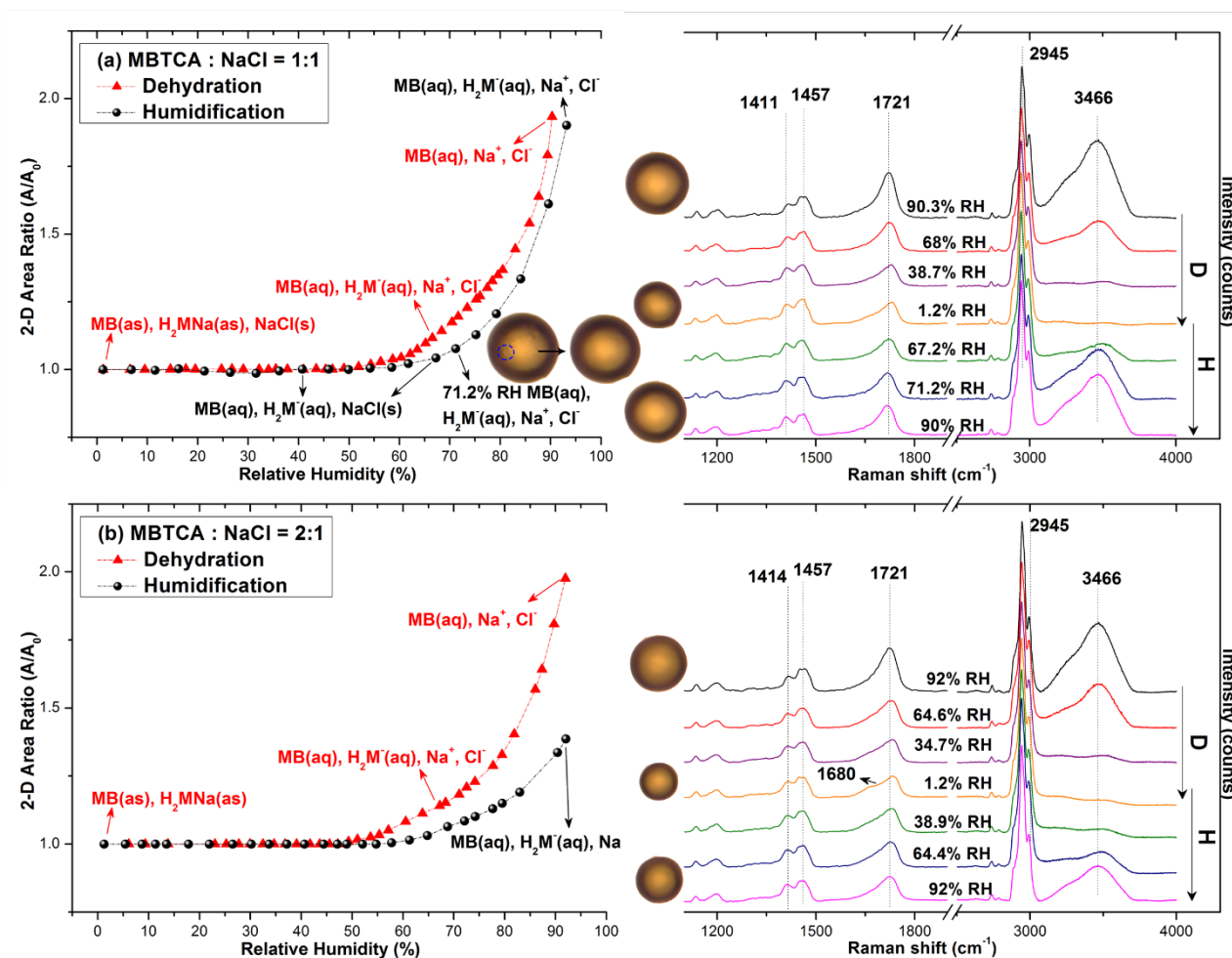


Figure 5. Hygroscopic curves, corresponding optical images, and Raman spectra at specific RHs of MBTCA:NaCl = (a) 1:2 and (b) 1:3. The recorded transition RHs during the dehydration (D) and humidification (H) processes and the chemical compositions of the mixtures at certain RHs are marked with arrows in the hygroscopic curves. The phase notations shown in parenthesis are s=solid; aq=aqueous; and as=amorphous solid.

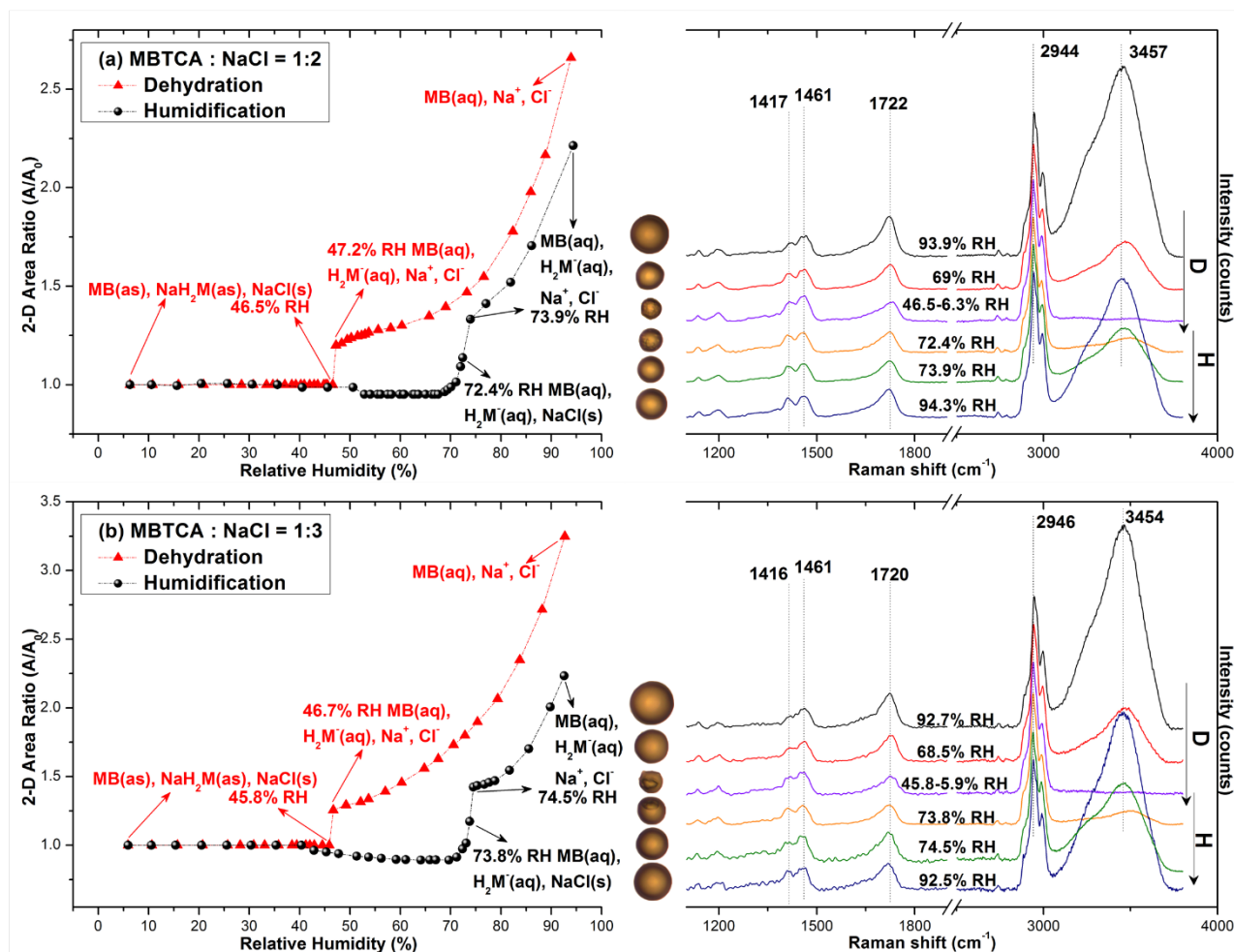
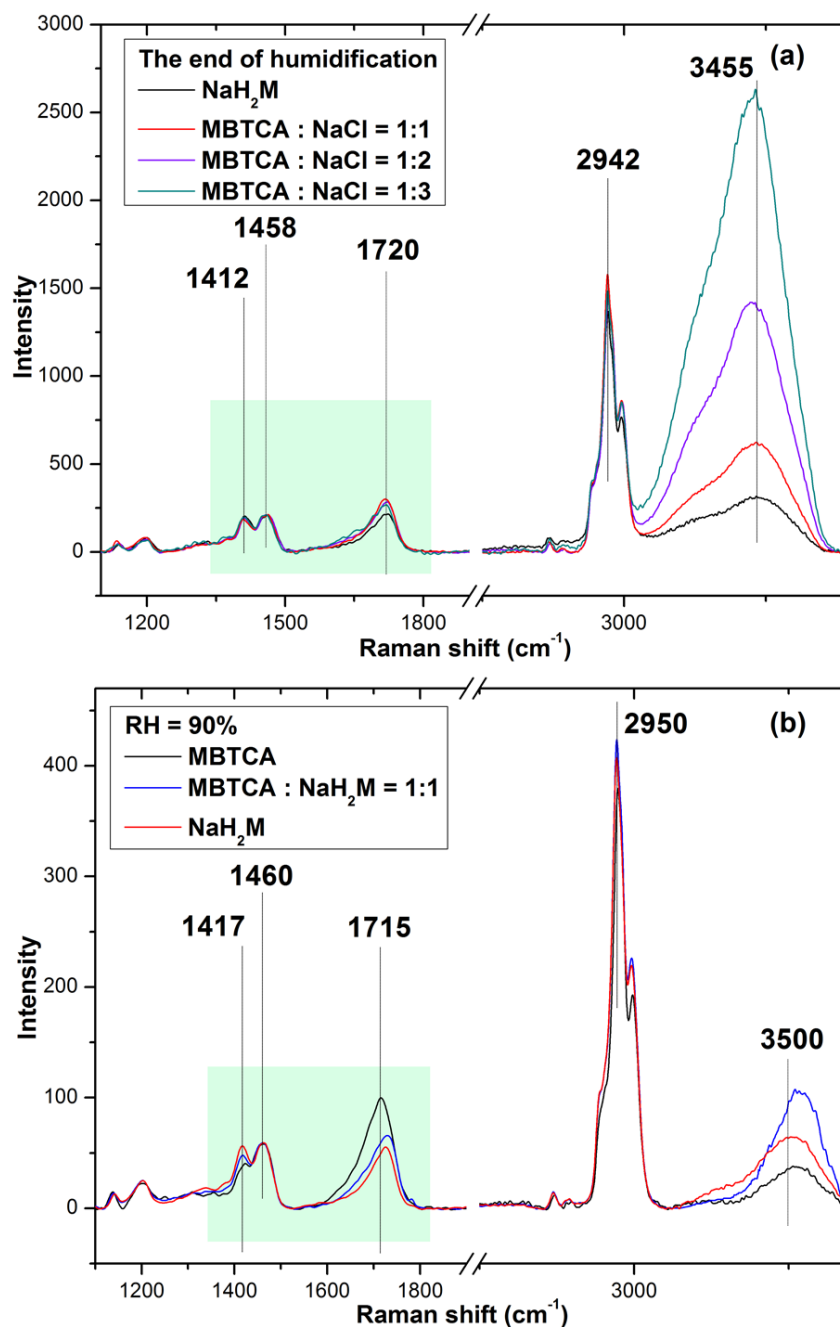
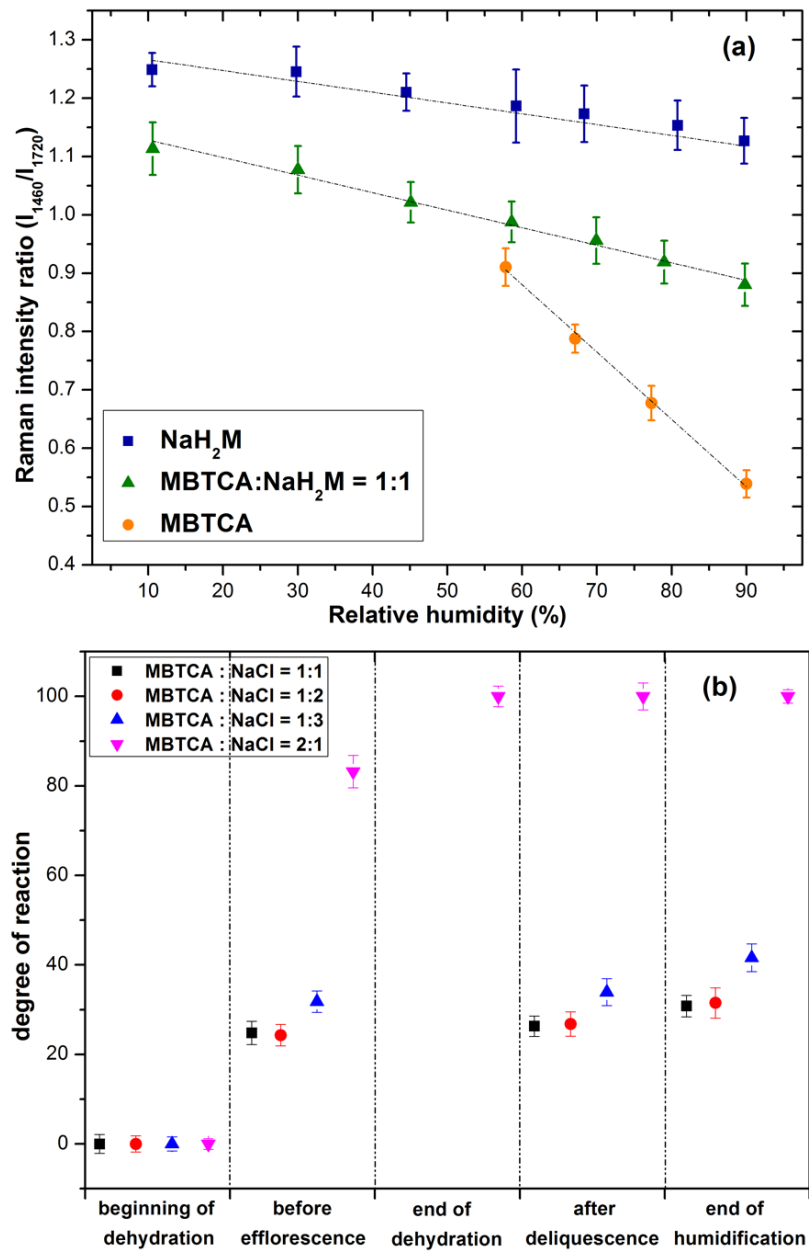


Figure 6. (a) Raman spectra of pure NaH_2M and mixture aerosols with mixing ratios of MBTCA: NaCl = 1:1, 1:2, and 1:3 obtained at the end of the humidification process, which were normalized to the CH_3 peak at 1458 cm^{-1} and (b) Raman spectra of pure MBTCA, mixture of MBTCA: NaH_2M = 1:1, and pure NaH_2M , which are normalized to the CH_3 peak at 1460 cm^{-1} .

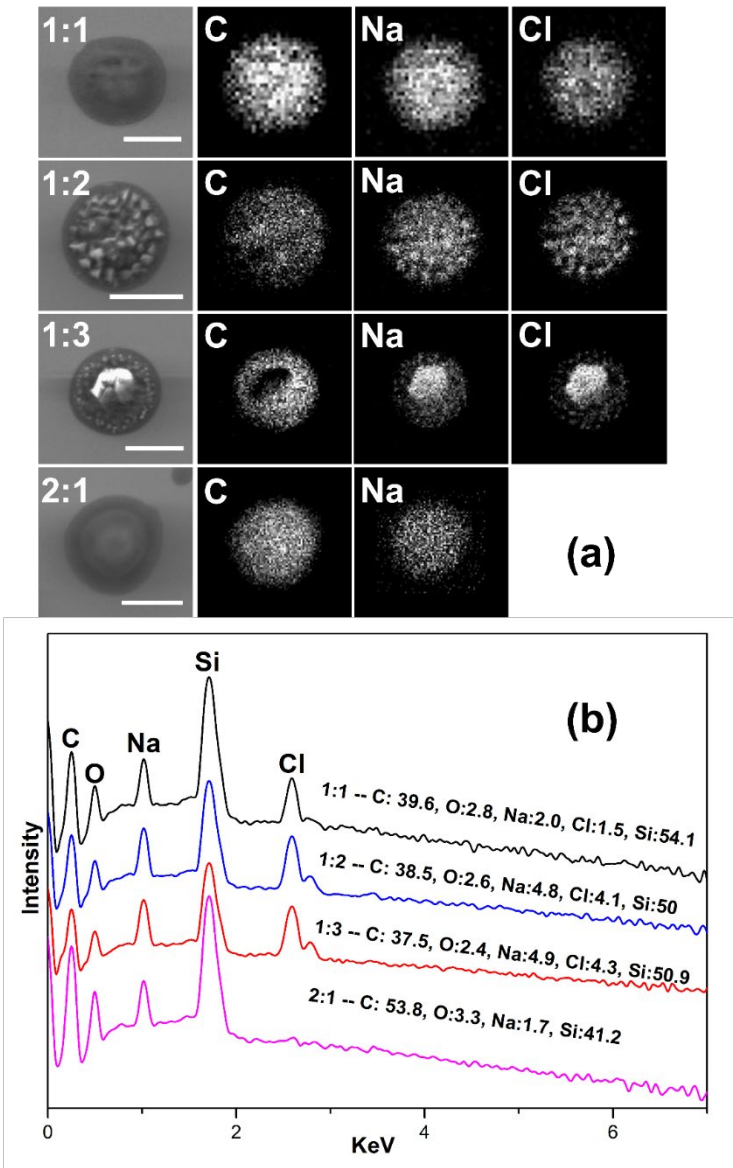


1037
1038
1039
1040
1041
1042

Figure 7. (a) Calibration curve calculated from the intensity ratios of two peaks at 1460 and 1720 cm^{-1} as a function of RH for NaH_2M , $\text{MBTCA}:\text{NaH}_2\text{M} = 1:1$, and MBTCA aerosols; (b) chemical reactivity represented as the degree of reaction for mixture aerosols of $\text{MBTCA}:\text{NaCl} = 1:1, 1:2, 1:3$, and $2:1$ during the dehydration and humidification processes.



1043 Figure 8. (a) Secondary electron images (SEIs) and elemental X-ray maps for C (from MBTCA and
1044 NaH_2M), Na (from NaH_2M and NaCl), and Cl (from NaCl). The scale bars are for 5 μm ; (b) X-ray spectra
1045 and elemental concentrations of particles with four mixing ratios.
1046
1047



1048 Figure 9. Hygroscopic curves, corresponding optical images, and Raman spectra at specific RHs of MBTCA:NaCl = (a) 1:1, (b) 1:2,
 1049 and (c) 1:3 mixture particles in the levitation system. The recorded transition RHs during the humidification (H) and dehydration
 1050 processes and the chemical compositions of the mixtures at certain RHs are marked with arrows in the hygroscopic curves. The phase
 1051 notations shown in parenthesis are s=solid; aq=aqueous; and as=amorphous solid.
 1052

